Applying Biomimetic Passive Dynamics to a Quadruped Robot Leg

by

Emma Krnacik

A thesis submitted in partial fulfillment of the
requirements for the degree of

Master of Science
in
Mechanical Engineering

Thesis Committee:
Alexander Hunt, Chair
David Turcic
Chien Wern

Portland State University
2022

Abstract

The study of synthetic nervous systems is an emerging field within biomimetic robotics as an alternative to more classic control techniques. As the modeling of these nervous systems becomes more accurate, it is important to note that the nervous system and physical system co-evolved and continue to operate in an interdependent fashion. Many legged robots, including the existing quadruped in the AARL, have leg systems that may have similar geometrical properties to that of a mammal, but have significantly different dynamic properties. This paper presents a method for designing a limb so that the passive dynamics more accurately represent that of mammalian limbs. The desired limb dynamics were obtained by scaling kinematic rat leg data, and a gray-box optimization method was used to determine appropriate spring and damper properties, modeling the limb as a three-link pendulum with a spring-damper system at each joint. The new leg was designed with minimal changes to the current prototype, with the implementation of a modular spring and damper set, which allows the leg to achieve more biomimetic passive dynamics. This leg was built with the intent of comparing SNS control methods on legs with different dynamic scales (i.e. inertial vs overdamped). Future improvements to the spring/damper implementation will include increasing the modularity of the mechanical design in order to more easily change the leg dynamic properties.

Acknowledgements

I would like to thank Dr. Alex Hunt for his guidance and mentorship on this project, as well as Dr. David Turcic and Dr. Chien Wern for serving on my thesis committee, providing feedback, and sharing their own experience in system identification and mechanical design. I'd also like to acknowledge the Portland State Agile and Adaptive Robotics Lab members, particularly Cody Scharzenberger for always being willing to share his time and experience, Stu McNeal for his programming expertise and guidance, and Ben Bolen, Manuel Mansilla, and Jason Miranda for aiding in equipment troubleshooting. This work was supported by NSF DBI 2015317 as part of the NSF/CIHR/DFG/FRQ/UKRI-MRC Next Generation Networks for Neuroscience Program.

Table of Contents

List of Tables

List of Figures

Chapter 1: Introduction

1.1 Motivation

The study of synthetic nervous systems (SNSs) is an emerging field of research in robot control [1]–[3]. Several recent studies have specifically focused on using synthetic neural networks to control legged locomotion [4], [5]. Legged locomotion is a prime example of the importance of form-function relationships, and as such, it is imperative to build a system that is biomimetic not only in control, but also mechanically. It is the intent of the AARL to study SNSs in systems that more closely mimic animal anatomy.

To investigate alternatives to classical control methods, the AARL has designed a quadruped robot with braided pneumatic actuators (BPAs) as a tool for synthetic nervous system research (Fig 1) [6]. The robot is an updated version of the Puppy quadruped robot from Case Western Reserve University, and structurally features a 3D printed frame (using Onyx from Markforged [7]) and 3-DOF legs actuated by 10mm BPAs from Festo arranged in antagonistic extensor/flexor pairs [8]. D-shaped steel rods are used as rotary shafts to connect limbs. Limb lengths and joint range of motion in the legs were remodeled to resemble actual canine anatomy. The future intent is to use SNSs to control coordinated locomotion using all four legs [6]. While the non-linear dynamics of the BPA's present a challenge to control with traditional methods, the force-length curves produced by these are a better representation of the dynamics of biological muscle function, when compared to motors or other actuator types. The biomimetic nature of BPAs is desirable as the robot is to be used as a tool to design biologically realistic

control methods. While BPAs more closely resemble an animal musculature system than a simple electric motor does, the dynamic properties of the robot leg itself do not resemble that of a canine, nor any other specific mammal. Hence, in order to design a biologically accurate and functional synthetic neural network controller, it is desirable to physically re-create a mechanical system with the same parameters as a given anatomical system to create a dynamically equivalent leg.

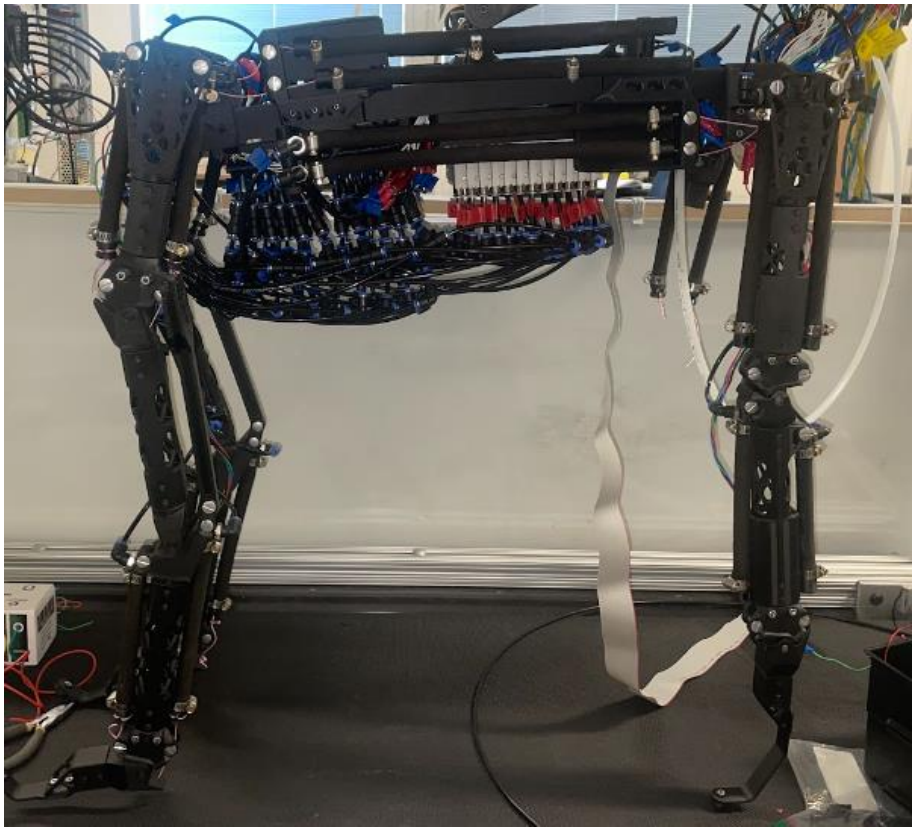

Figure 1: Current quadruped robot at the AARL at Portland State University.

As animal legs have been demonstrated to have varying dynamic properties depending on the organism, it is beneficial to reflect this in our study of synthetic neural networks. Through evolution, biological needs of the organism can dictate both

morphological and neural differences, and this can be observed in limb function. Limb dynamic behavior can be categorized as inertia-dominated, gravity/elastic force-dominated, or viscous force-dominated. It is important that neural control corresponds to the type of dynamic behavior the limb exhibits [9]. In order to implement proper control, the dynamic behavior of the limb must be identified and built in a testable system.

This thesis details the process by which limb dynamics of live animals were identified and how these dynamics were implemented in the dog robot. Using kinematic data collected from electrically stimulated rat legs by Dr. Matt Tresch from Northwestern University, the dynamic properties such as damping ratio and natural frequency were identified. The hypothesis driving this project is by using time-scaled rat hind limb data, a quadruped robot limb can be designed to capture the passive dynamics of an actual canine limb.

1.2 Overview

The workflow of this project can be broken up into three main stages: The mathematical modeling and designation of our leg system and optimization of dynamic parameters, the mechanical design of the scaled leg, and implementation and testing of the modified leg. Chapter two will cover necessary background information including the system representation for a quadruped hind limb, the derivation of equations of motion to model this system for this project, types of cost calculations used in the optimization process, and the electrical system used for limb testing. Chapter three will delve into the optimization of spring and damping parameters for the rat leg data. Chapter four will

discuss how these results informed our decision to appropriately scale for increase in length of the dog leg, and how the results from this were implemented into the new limb design. Chapter five will include and overview of the testing of the new limb, and a discussion on the new leg passive dynamics as compared to the rat limb, the original robot limb, and our expected results. Much of the success of the mechanically designed leg will be highly dependent on accurate modeling of a leg system and a robust identification of the dynamic system desired. A discussion on the efficacy of this process and potential applications in future biomimetic robotic research can be found in chapter six, along with suggested improvements to be made to the leg design outlined in this project.

Chapter 2: Background

In order to identify system parameters (damping ratio and natural frequency), motion data must be analyzed. Analyses of behavior in the frequency domain often provide the most robust results, however, given the biological nature of our system of interest, this method has many barriers. Designing and carrying out animal experiments presents an array of logistical hurdles, the most pressing of which in our case centers around lack of access. The quadruped robot is modeled after a medium sized dog, which would be difficult to obtain data on limb dynamics, as the animal would have to be anaesthetized and the AARL is not equipped for animal experimentation. This makes it necessary to turn to alternative methods.

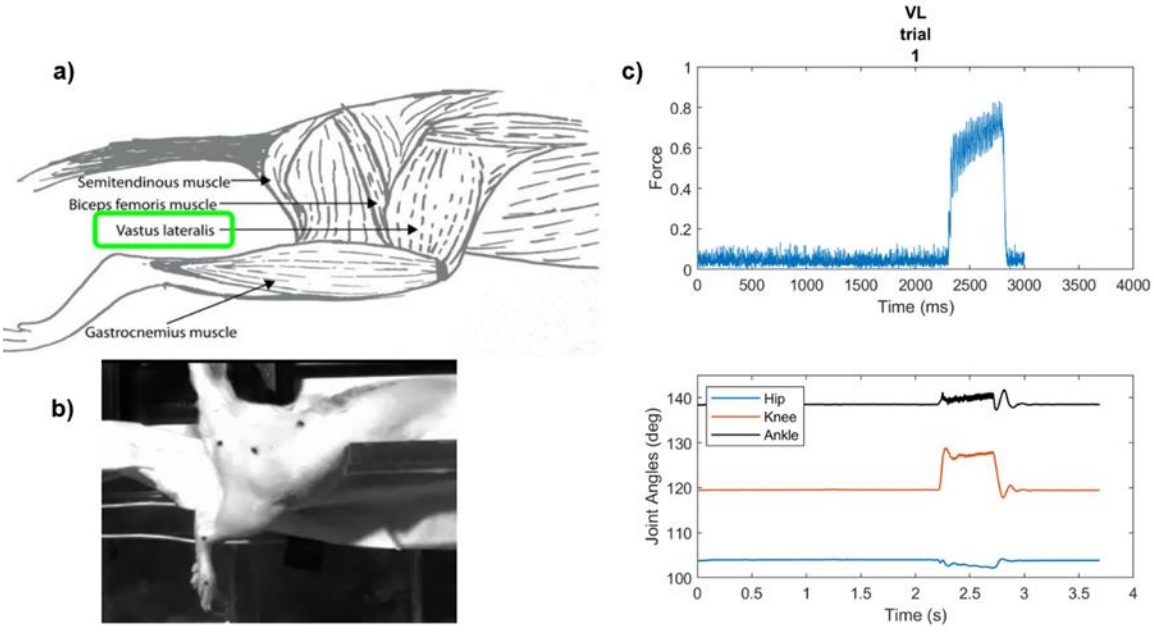

Figure 2: (a) Example image of the vastus lateralis muscle of the rat hind leg, corresponding to one of the stimulated muscle trials. (b) Image of anesthetized rat set-up for kinematic data collection. (c) Example trial of the vastus lateralis being stimulated, with corresponding normalized EMG force and joint angle response data.

Dr. Matt Tresch performed experimentation on the kinematic response of rat legs given an electric stimulus to hind leg muscles (Fig 2). In the experiments, rats were anaesthetized, an individual leg muscle was stimulated for a short period, and then released. Positional data was recorded before, during, and after stimulation. This process was repeated for seven different muscles in the rat hind leg, including the iliopsoas, gastrocnemius, semitendinosus, vastus lateralis, and biceps femoris (anterior and posterior) [10]. The processed positional time-stamped data was collected in the form of the hip, knee, and ankle joint angle data over time. The data was isolated to the time period directly after the electric stimulus was released to facilitate analysis of this data as a step response to a positional input (Fig 3).

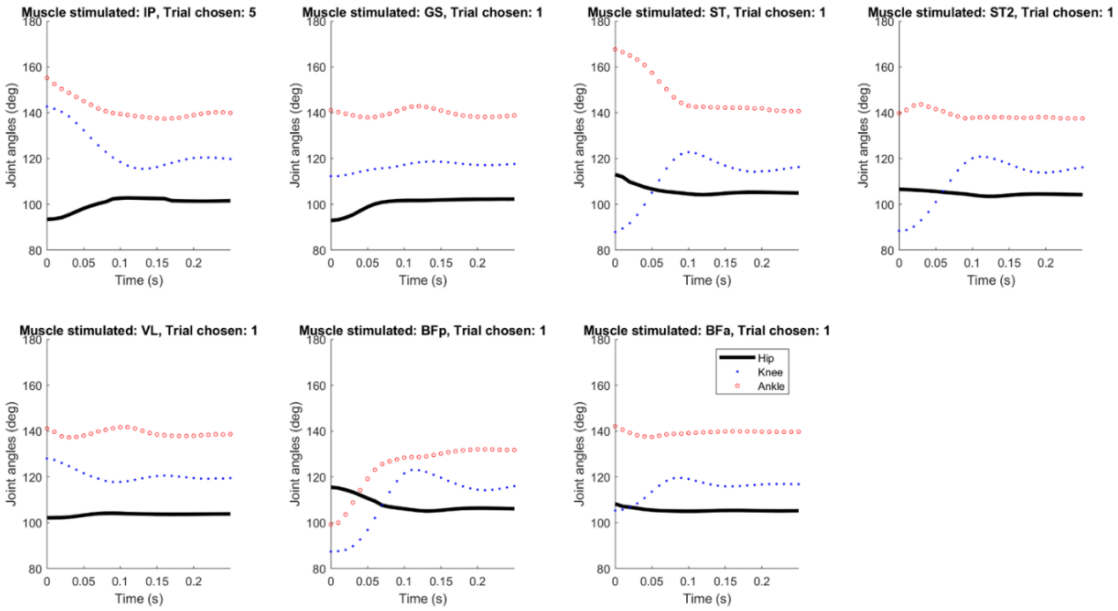

Figure 3: Isolated rat leg joint angle response to different positional inputs.

We then used a gray-box model to determine unknown parameters of the system. To do this, we first derived general equations of motion of the leg using the Euler-Lagrange

formulation. Then, we ran an optimization process to determine unknown spring and damper values for the joints. The first step in this process is to define the system as accurately as possible while also realizing that some assumptions and simplifications must be made while generating the model.

2.1 System representation

The rat leg and following modeled quadruped hind leg systems were simplified to a 3-link pendulum with a singular rotational joint at the hip, knee, and ankle (Fig 4). For the rat, geometric and mass data were provided by Dr. Matt Tresch, including link lengths, link masses, and center of mass location for each link. Joint angles were given at the hip, knee, and ankle as θ_1, θ_2, and θ_3, respectively.

In order to model system dynamics, rotational spring and damper pairs were assigned to each of the three joints, with unknown coefficients and unknown joint offsets at which each of the springs are unloaded.

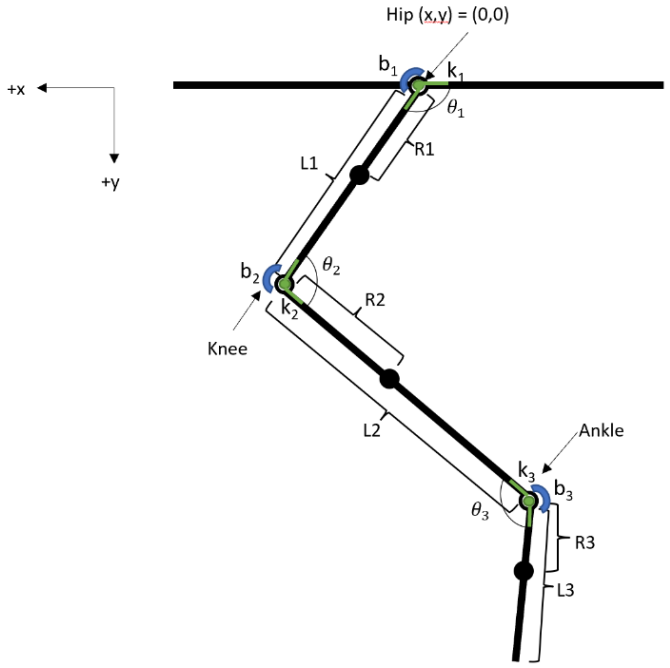

Figure 4: Schematic of leg system model, with designated mechanical parameters.

2.2 Equations of motion derivation

As the future goal of this research is to be able to test developing synthetic nervous systems on limbs with varying passive dynamics, it is advantageous to create a repeatable process so that other systems can be designed moving forward. In order to create a modular system optimization workflow, a general system of equations had to be derived. This was accomplished by using the Euler-Lagrange equations for a three-link limb with one degree of freedom at each joint [11].

$$\tau = \frac{d}{dt}\frac{\partial \mathcal{L}}{\partial \dot{\theta}} - \frac{\partial \mathcal{L}}{\partial \theta}$$

Equation 1

The Lagrangian is defined as the following:

$$\mathcal{L}(\theta, \dot{\theta}) = K(\theta, \dot{\theta}) - P(\theta)$$

Equation 2

Potential and kinetic energy are defined by the summation of each at each of the three links, where P_g and P_k refer to gravitational and spring potential energy, and K_t and K_r refer to translational and rotational kinetic energy, respectively.

$$K = \sum_{i=1}^{3} K_{t_i} + K_{r_i} \qquad P = \sum_{i=1}^{3} P_{g_i} + P_{k_i}$$

Equation 3

Additionally, a value θ_{bias} is calculated to represent the angle at which the spring at each joint is unloaded. This represents the 'resting' location for each joint when no muscle activation or external forces (such as gravity) are acting on it. This was found using the final resting position and calculated torque from gravity at each joint. These equations were then described and solved in MATLAB and saved as symbolic variables to be used in the optimization process.

Validation of the transient state of the model without spring and damping constants was completed checking the frequency of the leg locked out as a single link and comparing that value to known pendulum natural frequencies given a link of a specific length. The static state of the model (dependent of the unloaded spring angle calculation) was verified by running the equations of motion through the ODE function on MATLAB, given an arbitrary but realistic set of spring and damper values and initial angle positions. The static state of model was compared to the expected resting state based on the rat leg data provided (Fig 5).

Due to the length, the entire derivation of the model is not described here in detail, but can be found on the AARL GitHub repository: https://github.com/Agile-and-Adaptive-Robotics/Quadruped_Robot/tree/DampedLeg_Krnacik.

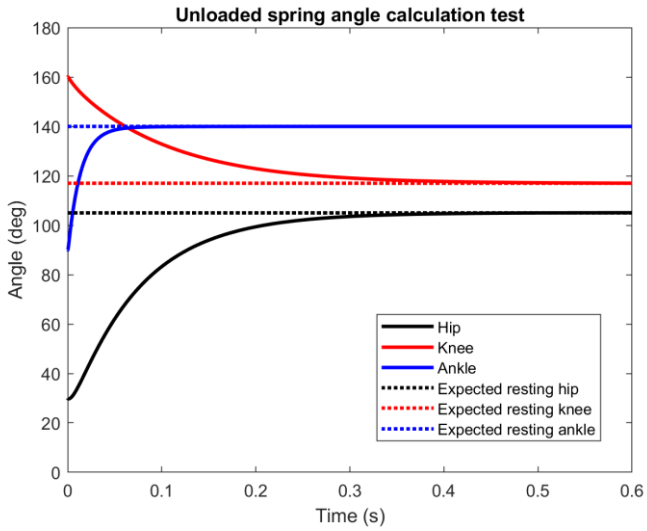

Figure 5: Model validation for correct calculation of the unloaded spring value.

2.3 Methods of cost calculation

There were two primary ways in which cost was calculated in the optimization phase of this project. The first method used was a root mean square between each actual and theoretical joint angle at each time point:

$$cost = \sqrt{\frac{\sum_i^n err_i^2}{n}}$$

Equation 4

Here, cost represents the cost of each search iteration of a given trial with a single set of parameters, where n is the total number of time points, and err is the difference between actual and desired joint angles.

Another type of cost calculation that was used directly compares specific qualities of the transient state of the joint response, which included rise time, damping ratio, and damped frequency. Rise time was calculated by measuring the time it took a given joint angle response to travel from 10% to 90% of its steady state response, where the initial joint angle value to the steady state response were scaled as a measure from 0 to 1.

Damped frequency was calculated by measuring the inverse of the time it took for a response to oscillate from peak to peak. This calculation was only used on responses that had clear and defined oscillation periods.

The damping ratio, which was also only used with trials with clear and defined oscillation periods, was calculated using the logarithmic decrement:

$$\delta = \frac{1}{n} ln\left(\frac{x_1}{x_{n+1}}\right)$$

Equation 5

Here, x represents the amplitude of a given peak, while n represents the order of consecutive peaks. This was related to the damping ratio in the following way, assuming ζ is larger than 0.1:

$$\zeta = \frac{\frac{\delta}{2\pi}}{\sqrt{1 + \left(\frac{\delta}{2\pi}\right)^2}}$$

Equation 6

Each of these given qualities were used in the cost calculation by taking the scaled difference between actual and theoretical values, and if multiple qualities were being used, the cost was a summation of these scaled differences.

2.4 Quadruped test bench set-up

For the mechanical testing of the novel leg, the limb was affixed to a test bench so as not to interfere with the current quadruped prototype (Fig 6).

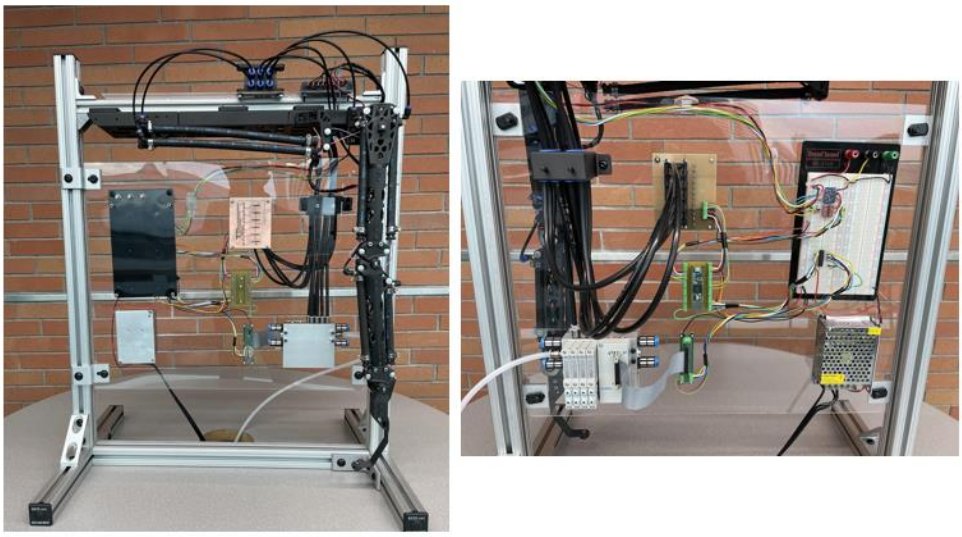

Figure 6: Quadruped test bench set-up.

An AMT103-V encoder is affixed to each rotary shaft to collect joint angle positional data over time. A bi-directional logic level converter board is used to reduce the 5V output from the encoder to 3.3V, so that the signal can be read by a 4.1 Teensy microcontroller (Fig 7). The test bench is also equipped for pneumatic actuation but was

not utilized for this project.

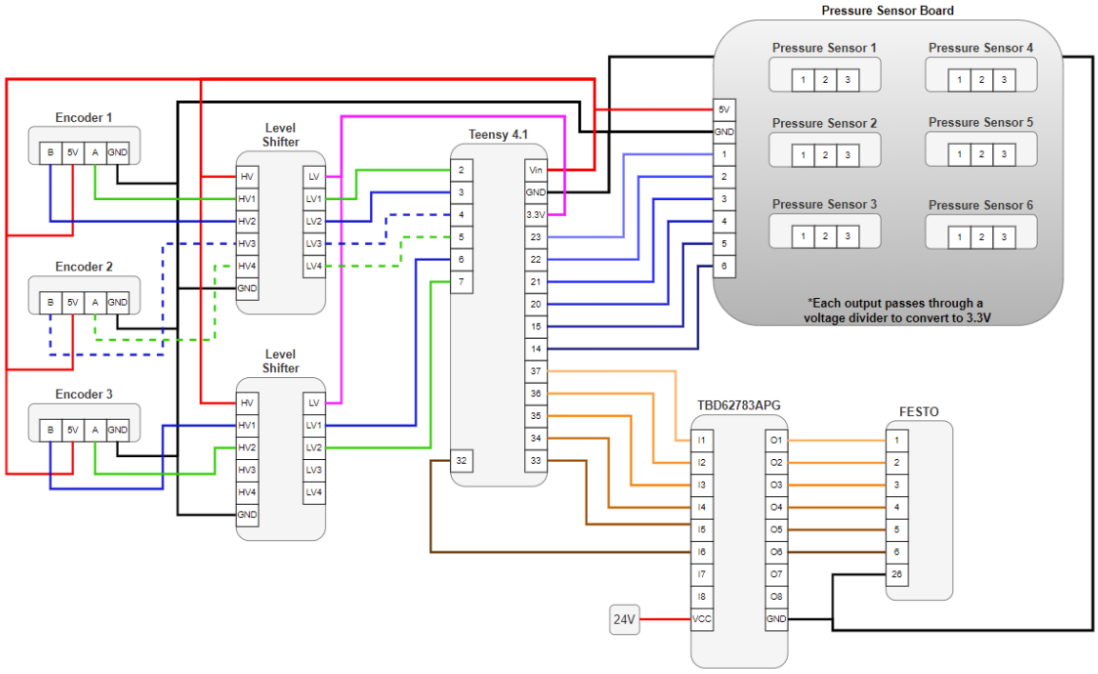

Figure 7: Wiring schematic for the quadruped test bench.

Chapter 3: Modeling of a rat leg

Chapter three will cover the initial phase of this project. This will include the methods used in the rat leg system identification, the results of this optimization, and a discussion about the final identified system and comments on the workflow process.

3.1 Methods

After the general equations of motion of the leg are defined, we can begin our system identification by utilizing a gray-box model with parameter optimization. Former AARL member Joseph Sammartino built a foundation for this optimization process using a Nelder-Mead search algorithm and educated initial guesses to solve for all parameters simultaneously [12]. The ODE function in MATLAB was used to model responses given initial joint angle conditions from each trial, using the previously derived EOM and initial search parameters for damping and spring values (Fig 8).

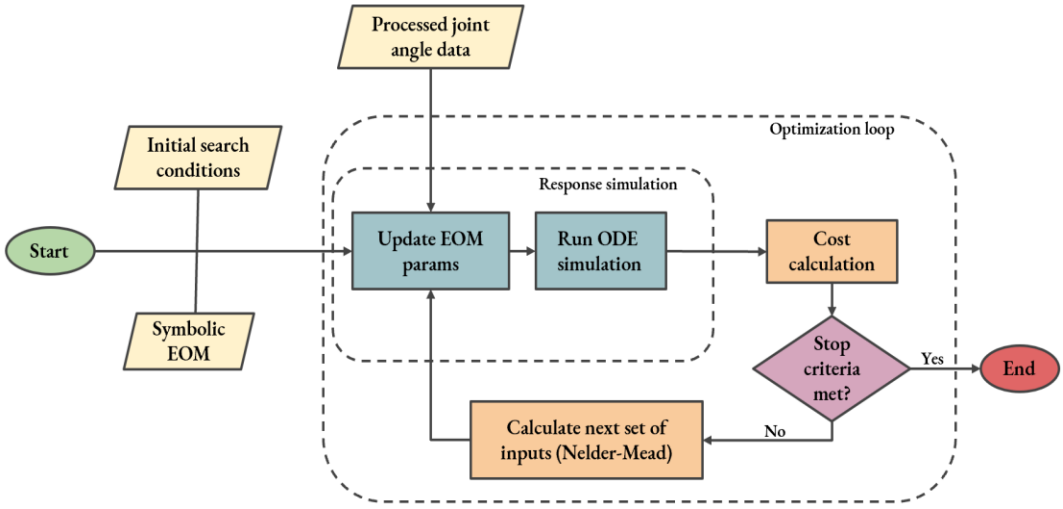

Figure 8: Workflow diagram of optimization process used.

The results (as time, joint angle, and joint velocity) were then compared to the actual processed joint angle data for each respective muscle trial (seven in total) as a cost calculation. Initially, the cost was calculated by a summation of the root mean square of the error between each actual and theoretical joint angle at each time point. This cost calculation was not effective, and changes were made to the cost calculation that will be discussed shortly.

The Nelder-Mead algorithm is then used to update search parameters, and the loop repeats until the stop criteria is met. The output of this process are optimized values for the spring and damping constants at each joint. This report will address some improvements to this method, as well as search method validation.

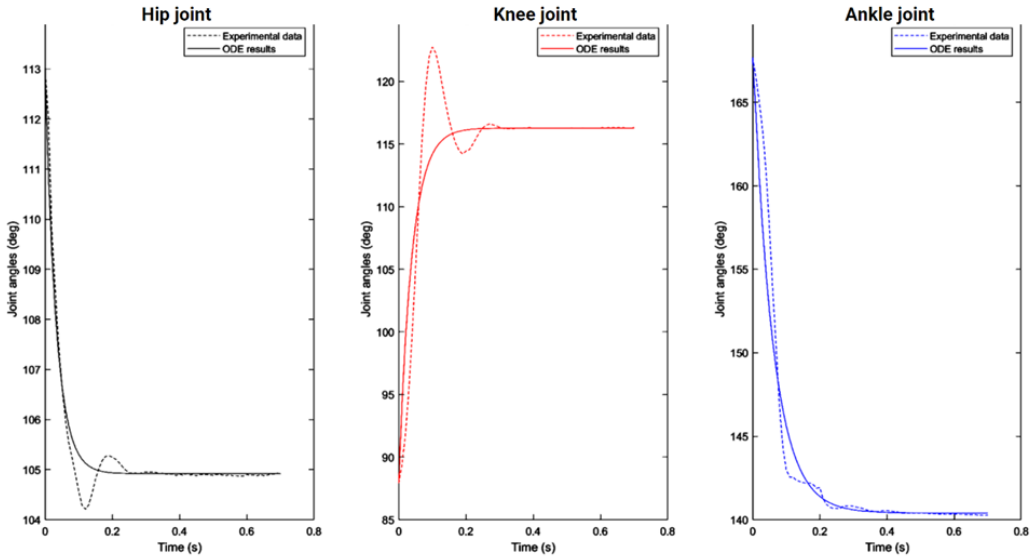

Figure 9: An example of an early-stage optimization results for a specific trial in which a local minimum where the theoretical system is overdamped was found.

The first and most persisting challenge throughout this project was the presence of many local minima. Specifically, in this system many local minima exist resulting with

overdamped systems (Fig 9). To address this issue, the first approach was to implement a broader set of solutions aimed at reducing the occurrence of local minima in the solution space.

First, we were able to give the search function more educated initial conditions by creating a short MATLAB script that allows the user to assign spring and damper values for all joints, and given a specific muscle trial, will output the response of the theoretical system as compared to the selected trial. If a joint was obviously underdamped or overdamped, the damping and spring constants were adjusted accordingly until the output of the theoretical system began to mimic the actual response. The spring and damper values used for this were then saved and used as starting search conditions in the optimization. Using this same script, approximate boundary conditions for the search could also be applied as it became apparent for each joint that parameters outside of a certain range would not give accurate results. Additionally, in order to emphasize the importance of the accuracy in the transient state, the error in joint angles at time points during the transient state (approximately 0.2 seconds) were given a higher cost by assigning a scalar multiple to the error in these data points.

Generally, this first set of solutions did reduce overdamping, but it still produced unsatisfactory responses in the transient state. One reason for this is that the set of joints are highly interdependent and the movement of each joint is dependent on the motion of the joint above it. This can cause incorrect parameters in one joint to adversely affect the behavior of another joint, and differences between theoretical and actual hip data will

cause in error in the knee and ankle, even if the parameters for those joints were chosen correctly.

Two things can be observed about the interdependence of the three joints. First, the mass of the third link is low relative to the mass of the first and second links. As such, the movement of joint three has very little effect on the movements of both joint one and two. Second, the masses of link one and two are quite similar to one another, and both have a significant effect on the response of the other.

Although we do not have the freedom to test different leg position inputs at will, the data used for this project recorded the response to multiple stimulated hind leg muscles, providing a total of seven different system inputs. Several of these results have a small to negligible hip input, which provides an opportunity to isolate the response of the knee, as the effect of the ankle on the knee is minimal (Fig 10).

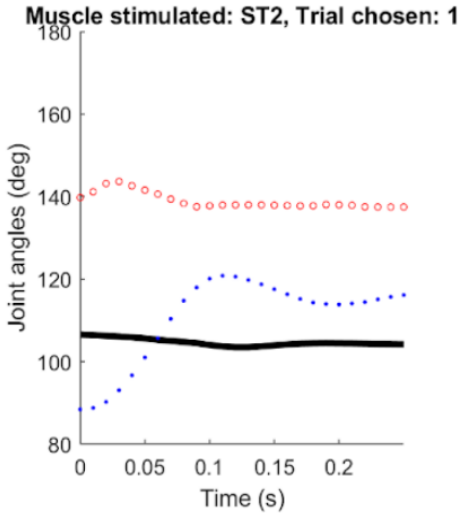

Figure 10: Example of trial with minimal hip input used in piecewise knee optimization.

Noticing this, a piecewise optimization was implemented. Four data sets with negligible or overdamped hip responses were used to optimize for the knee only, and the error of each of these responses was used in calculating the cost for each optimization iteration with a single set of parameters. The values for the hip and knee were hand set to reasonably account for each joint behavior and were left constant during the optimization process.

This method improved the results of the optimization, however the issue of overdamping still lingered. Reflecting on what characteristics are important to mimic in the system, the cost calculation in the optimizer was adapted to directly solve for these values. Initially, the optimizer used a simple mean-square calculation to assess error between the simulated and actual responses. The issue with this, is the overdamped solution is almost always the closest local minima because for any spring value chosen, there are an infinite number of damper values associated with it that produce an overdamped system. The search function then ends up trying to create an approximation of the curve path that doesn't replicate important passive dynamics.

Observing the knee data, the most relevant parameters to match are the damped frequency and the damping ratio. The cost calculation was modified to calculate for the difference between these values directly. This proved to be the most effective method.

Continuing with this piecewise optimization method, the values found for the knee optimization were then fixed, and the same process was run on the hip. However, the hip response is generally overdamped, and does not contain significant overshoot or oscillations. This made it necessary to use rise time instead of damping ratio and

frequency as a measure of error. After this, the ankle optimization was run keeping hip and knee values constant. Similar to the hip, the foot does not exhibit much oscillation and the cost calculation for this stage was a mean-square error calculation.

Although the above "piecewise" optimization method worked reasonably well in terms of results found, this process was specific to our data set used and a more robust method of optimization is desirable. For this reason, a particle swarm optimization was run to validate the results of the piecewise optimization, with the intent to replace the piecewise optimization with a more versatile process in future applications [13]. 100 iterations were run with 20 particles, and the optimization results from the piecewise optimization were used for a single starting particle in the particle swarm optimization. The same type of cost calculation was used for each joint and trial.

3.2 Results and validation

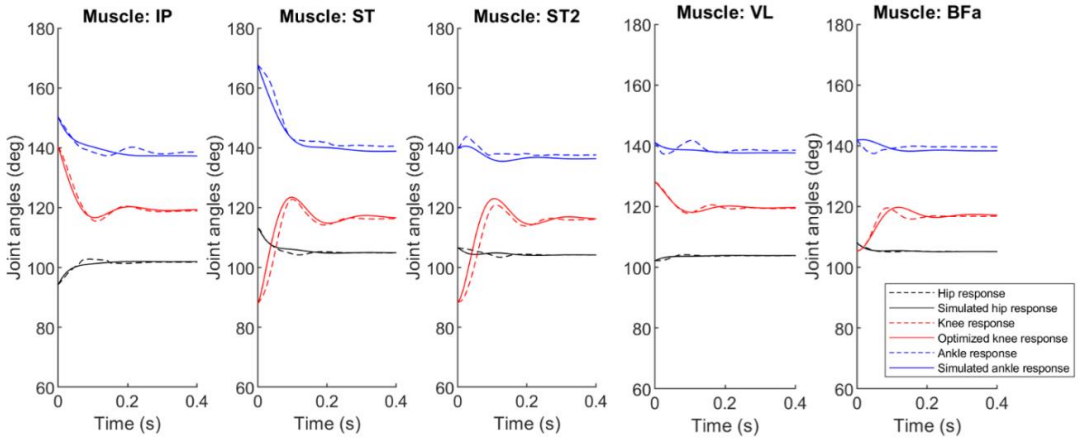

Figure 11: Results of knee optimization, comparing simulated and actual responses for trials used in the optimization.

The knee optimization resulted in in less than 20% average difference in damping and frequency values with a knee input greater than 10 degrees. As can be somewhat expected, this discrepancy tends to increase with lower knee inputs, due to lower signal to noise ratio (Fig 11).

All six parameter outputs from both the piecewise optimization and the particle swarm optimization are shown in table 1. On average, the results from the particle swarm optimization varied by approximately 14%. Table 2 summarizes the success of identifying the dynamic characteristics of interest for both processes.

Spring/damper parameter optimization results						
	Hip (k1) mN-m/rad	**Hip (b1) mN-m-s/rad**	**Knee (k2) mN-m/rad**	**Knee (b2) mN-m-s/rad**	**Ankle (k3) mN-m/rad**	**Ankle (b3) mN-m-s/rad**
Piece-wise	3.43	117	0.216	8.01	0.108	1.51
P. swarm	3.77	124	0.150	6.32	0.117	1.37
Pct diff	10%	6%	31%	21%	8%	9%

Table 1: Simulated and actual response for all trials using piecewise optimization.

	Freq error (median)	**Damping error (median)**	**Risetime error (median)**	**Avg joint angle err (deg) (median)**
Piecewise	19%	29%	19%	2.23
Particle swarm	23%	22%	13%	2.27

Table 2: Accuracy of particle swarm optimization and the piecewise optimization as a measure of selected dynamic characteristics.

Results were visually compared and were overall quite similar, with some small differences that were more obvious in particular trials (Fig 12, 13). The most significant differences found were in the knee, where there was a 20 to 30% difference in parameters found between the piecewise optimization and the particle swarm optimization.

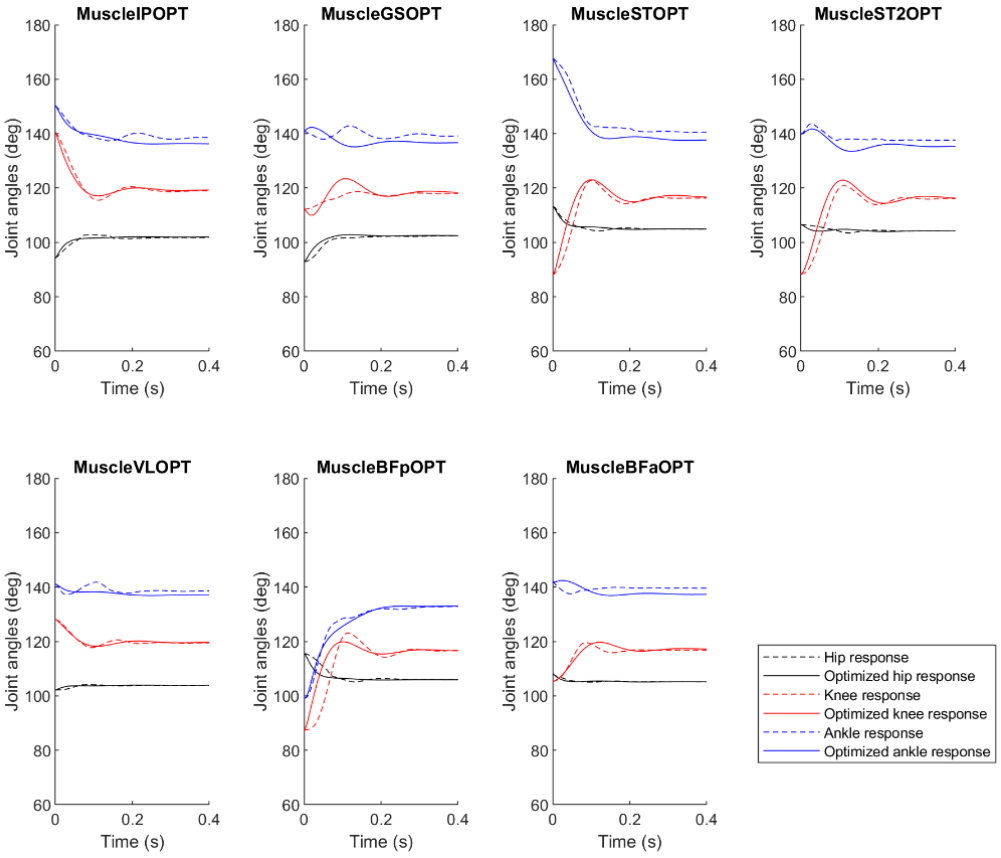

Figure 12: Comparing the simulated leg responses using the results of the piecewise optimization to the actual leg response data for all seven muscles stimulated.

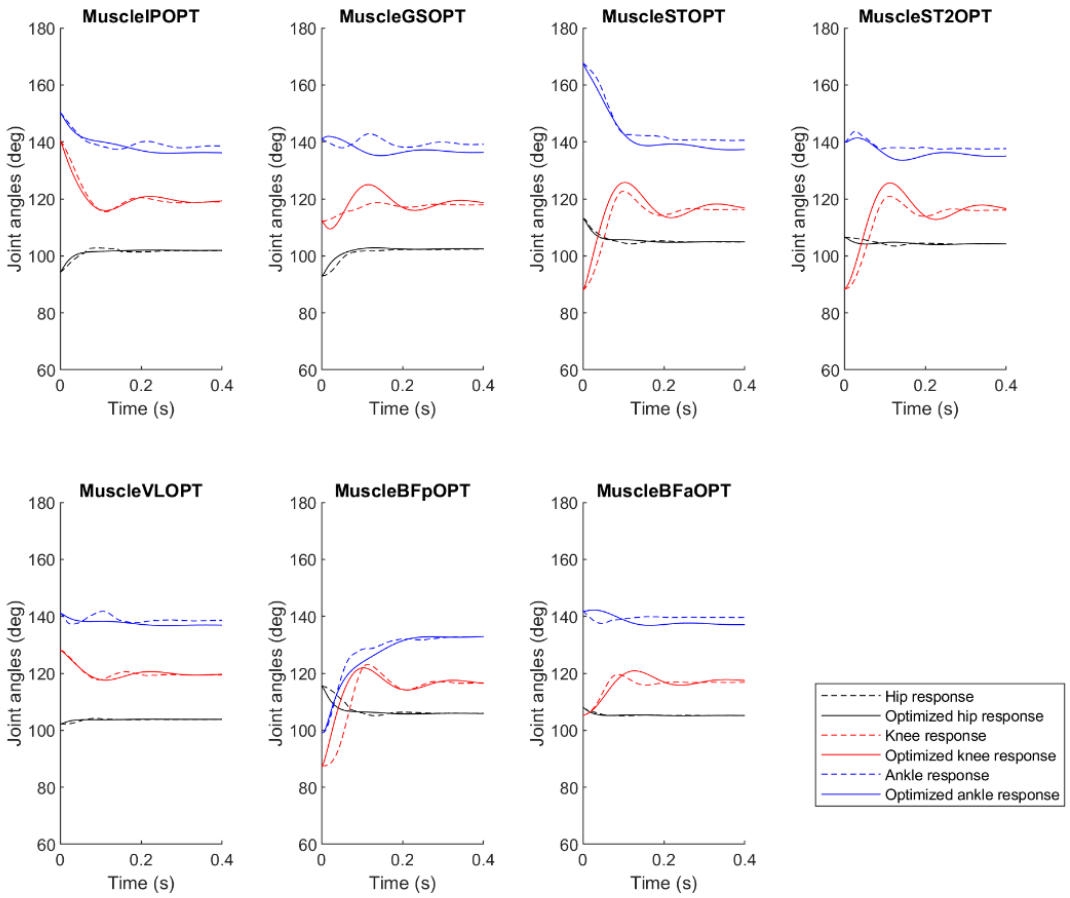

Figure 13: Comparing the simulated leg responses using the results of the particle swarm optimization to the actual leg response data for all seven muscles stimulated.

3.3 Discussion

Upon inspection, the piecewise results perform better in trials with significant knee movement, while the particle swarm optimization performed better on trials with less movement. For the robot leg optimization, trials with higher inputs (larger starting angles) for each joint were weighted higher, respectively, in order to put a focus on trials that exhibit a higher range of movement during optimization in order to ensure more realistic behavior for large motions like locomotion.

The success of both search methods were relatively similar, although each was more or less successful at identifying different parameters. It should be noted though, that the particle swarm optimization offers the ability to search many more parameters at a faster rate than the Nelder-Mead, while eliminating the issue of local minima, and is generally a more modular method. If the parameters to be searched is relatively small however, the Nelder-Mead approach is adequate and faster.

While it would be desirable to be able to reproduce the response of the rat leg to a higher degree of accuracy, it is important to acknowledge the limitations of this approach. A three-link pendulum with spring-damper pairs at each joint is a rough approximation of an actual rat leg. First, our study does not take into account any abduction or adduction movement from the rat leg. Each joint is assumed to have a singular degree of freedom, which is not true, especially in the hip and ankle. Second, our system has simplified torque exerted on the knee to either be due to gravity, spring force, or viscous damping. The physiology and structure of the rat limb may not strictly adhere to these types of torques, and the anatomy of the fascia and musculature will likely differ in mechanical properties than a spring-damper system. However, given these limitations it shows promise that the passive dynamics were able to be modeled in this way to some degree of success.

Chapter 4: Design of the quadruped leg

The optimization for rat leg dynamic properties serves as a useful process validation and as a starting model from which to begin modeling a dynamic dog leg. However, rat legs and dog legs do not operate on the same time scale. Therefore, in order to pick spring and damper values to implement accurate passive dynamics onto our dog-adjacent legs, the rat leg time-responses needed to be scaled appropriately.

We considered three different scaling options for this project, including capturing the passive dynamics of a rat in a dog-sized robot, the passive dynamics of a dog in a dog-sized robot, or the scaled passive dynamics of a rat in a dog-sized robot. The option to implement the passive dynamics of a rat in a dog-sized robot was dismissed as an initial prototype for this project due to the high torques that would be necessary to mimic the relatively fast rodent time scale. While general time scales for the strides of many quadrupeds have been estimated, there is very little data on specific parameters, such as damping ratio, or natural frequency for canine joints [9]. While these can be estimated, we found it most appropriate to mimic the scaled passive dynamics of a rat in a dog-sized robot. This chapter will outline how this was completed, and the design choices for the novel leg.

4.1 Robot leg scaling

Some assumptions and simplifications were made in adjusting the rat leg response data to a longer limbed quadruped. It was necessary to increase the time scale of the

response in accordance with known time scales for rat and larger quadruped strides. Data suggests rats have a walking stride period of 0.2 to 0.6 seconds, and medium sized dogs exhibit a walking stride of 0.75 seconds [9], [14].

Following this information, the collected rat data timescale values were adjusted to be twice their original value, and joint angle data was kept at the same amplitude. Doing so maintains similar properties such as overshoot and damping ratio, while decreasing damped and natural frequency. This new scaled data set was run through the optimization process outlined in chapter 3 with an updated set of geometrical properties measured from the robot leg, including masses, center of mass measurements, and link length measurements. This process was completed to obtain spring and damping values for the robot leg that would cause the passive dynamics of the robot leg to mimic those of the scaled rat leg response (Fig 14). Spring and damping values were recorded to inform the design of the torsion spring and rotary damper implementation (Table 3,4). Detailed results from the parameter fitting process can be found in the appendix.

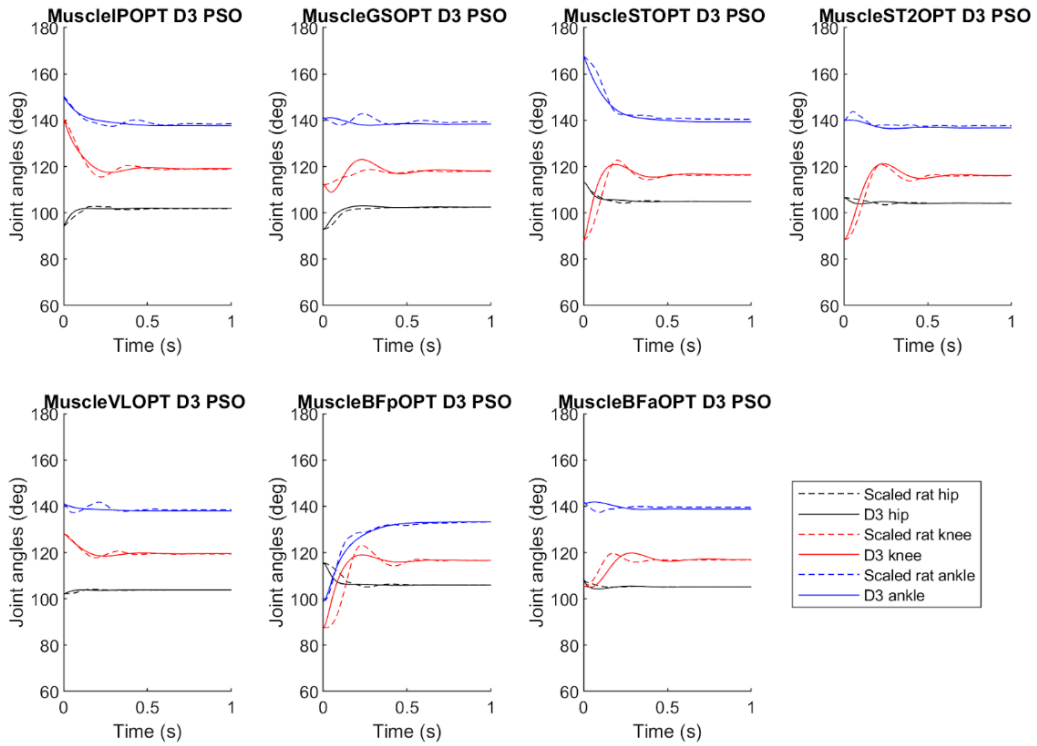

Figure 14: Comparing the simulated leg responses using the results of the particle swarm optimization to the actual leg response data for all seven muscles stimulated.

Spring/damper parameter optimization results					
Hip (b1) N-m-s/rad	**Hip (k1) N-m/rad**	**Knee (b2) N-m-s/rad**	**Knee (k2) N-m/rad**	**Ankle (b3) N-m-s/rad**	**Ankle (k3) N-m/rad**
1.29	23.7	0.105	1.71	0.063	0.454

Table 3: Parameter optimization results for the scaled rat leg.

	Hip	Knee	Ankle
Unloaded spring angle	105	108	139

Table 4: Values for the unloaded spring angles (θ_bias).

4.2 CAD modeling and design

In implementing the torsion springs and rotary dampers, there were two design goals to keep in mind. First, it is desirable to keep the additional spring and damper

components as modular as possible, as it is likely that other parameters for future leg versions will be made. Second, as the goal is to compare how this leg responds to a specific type of control relative to the original leg and possibly other variations, it is advantageous to keep the novel leg design resembling the original design (Fig 15).

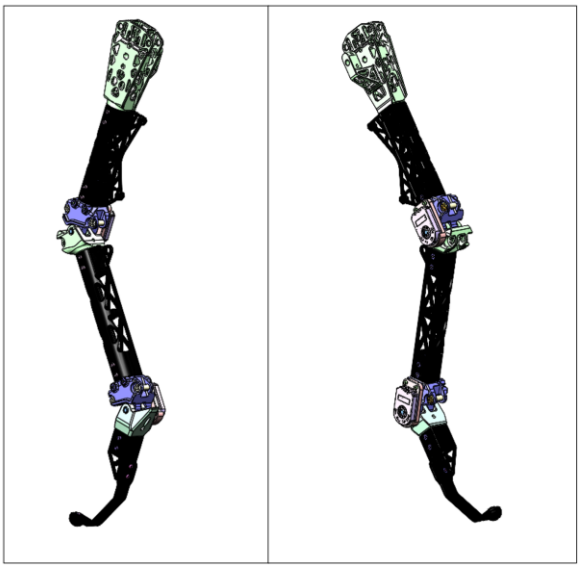

Figure 15: Original hind leg design on the quadruped test bench.

So, although these new components must be added, the goal is not to design an entirely new leg.

Due to their similar mechanics, the ankle and the knee were designed in parallel. All CAD models were created in SolidWorks. For both joints, a bracket was placed on the lateral side of the leg to hold the rotary damper in place relative to the upper joint, while the damper inserts into the lower joint piece to create torque as the joint rotates (Fig 16).

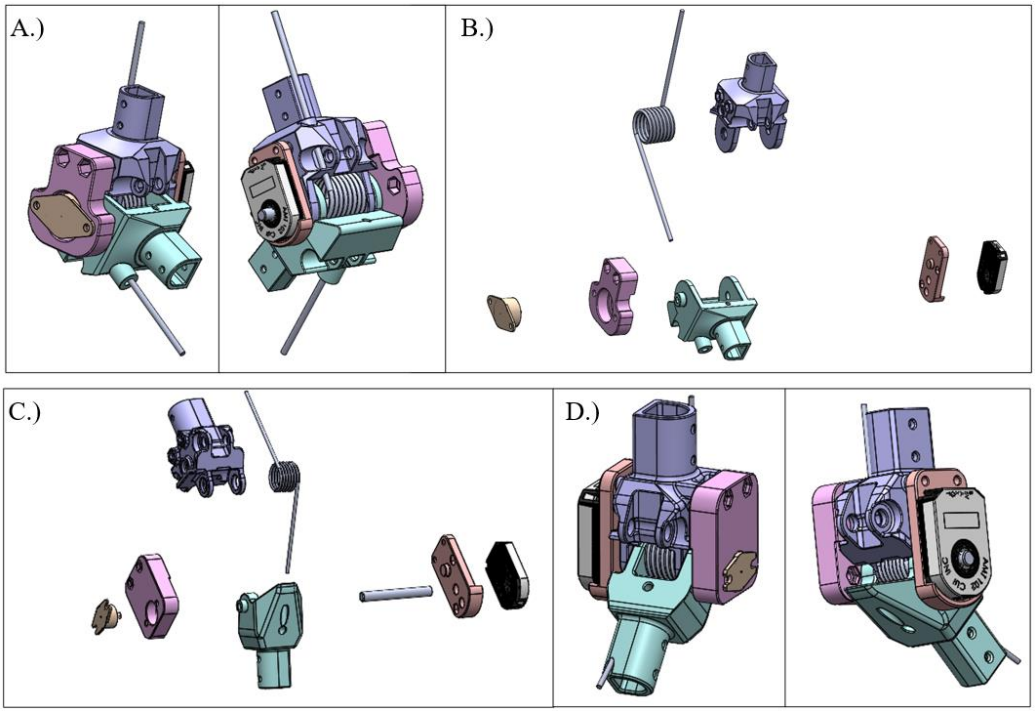

Figure 16: a.) Assembled final knee design in SolidWorks with medial encoder and lateral damper placement. b.) Exploded view of knee design. c.) Exploded view of finalized ankle design. d.) Assembled final ankle design in SolidWorks with medial encoder and lateral damper brackets.

As the damper and encoder are both installed on the lateral and medial sides of the joint respectively, it seemed advisable to place the torsion spring within the joint itself so as not to add more hardware to the external joint pieces. Due to the smaller width of the chosen ankle spring, this was accomplished by decreasing the hinge width of the ankle joints. The torsion spring for the knee joint however, is larger in width and diameter than the original knee joint capsule allowed for, so the knee joint was redesigned from scratch, retaining all original features but changing the scale. Most of note, the hinge diameter and width between the hinges were increased in the new design. The legs of the springs are held into place by shafts that enter into both the upper and lower joint pieces. The upper shaft for each spring runs parallel to the leg link, while the lower shaft was placed at an

angular offset to account for the difference in the 120-degree spring angle and the unloaded spring angle calculated in the optimization process (139 degrees for the ankle and 111 degrees for the knee).

The hip spring presented more of a challenge, as a pre-made spring heavy enough to mimic the spring value found in the optimization would introduce further protrusion from the body of the dog. However, due to the smaller range of motion necessary for the hip (15 degrees from one direction of the unloaded spring and 45 degrees in the other) we decided to make the spring for the hip using music wire using the design process outline in chapter 4.3.2. As the steel rod for the hip joint rotates with the leg, the damper was placed on the inside of the joint and an adapter was designed to attach the hip fin to the square damper insert. Shafts were added to the upper and lower hip joint to secure the spring legs to their respective pieces (Fig 17). CAD drawings for the joint pieces, dampers, and springs can be found in the appendix.

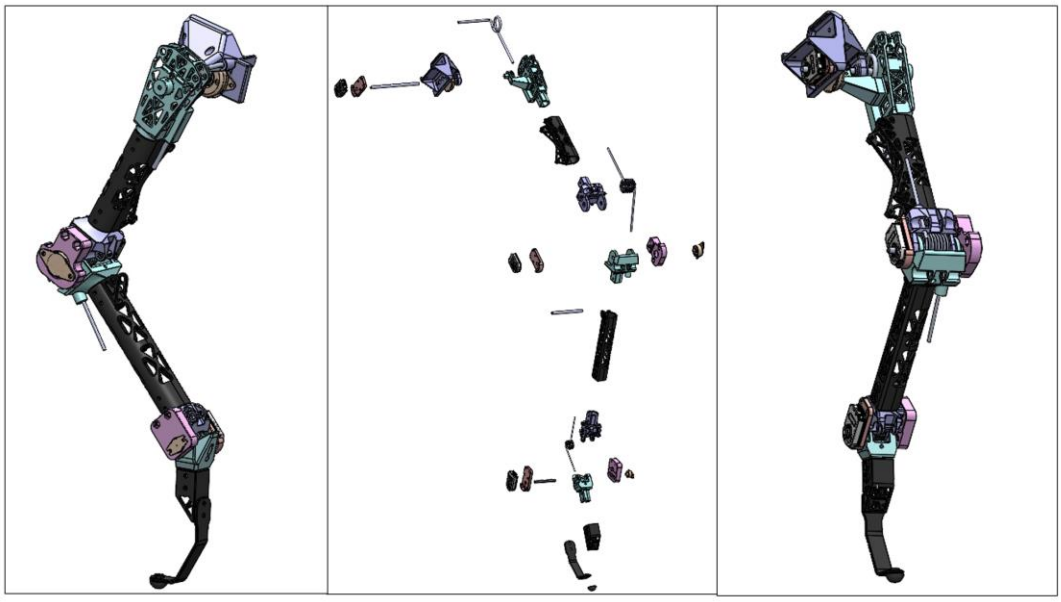

Figure 17: Final novel hind leg design in SolidWorks.

4.3 Spring and damper design choice

4.3.1 Damper design

Initially, rotary dampers were selected assuming they exhibited a linear relationship between angular velocity and torque exerted, as is the case in viscous damping (and in our model). This was completed by using the max torque and speed provided by the vendor and calculating the assumed slope of torque over angular velocity. However, this is not the case for most torsional dampers (Fig 18) [15]. This assumption caused our initial damper selection to be too strong, and the dampers were replaced with a set with a lower max torque (Table 5). Dual direction and 360-degree rotation dampers were used for all joints.

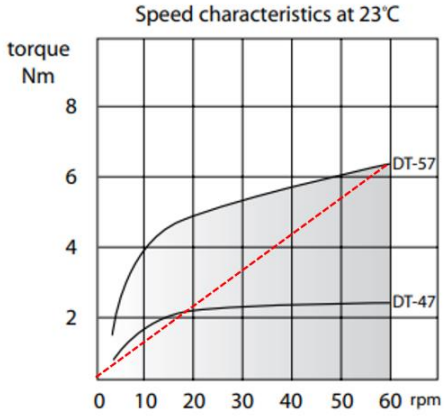

Figure 18: An example of a typical viscous damper provided by the ACE Rotary Damper Catalogue. Red dashed line depicts a linear relationship between angular speed and time, and the solid line indicates the actual damper specs.

Specifications	Hip	Knee	Ankle
Vendor	McMaster-Carr	McMaster-Carr	McMaster-Carr
Product number	6597K21	6597K19	6597K8
Max torque	312 in-oz	31 in-oz	7 in-oz
Max speed	50 rpm	50 rpm	50 rpm
Directionality	Dual	Dual	Dual
Rotation limits	360 deg	360 deg	360 deg
Force mechanism	Oil	Oil	Oil

Table 5: Product information on the rotary dampers at each joint.

After the dampers were installed on the robot leg, data was gathered on the new joint responses. The goal of this step was to identify the actual viscous damping occurring at each joint, instead of estimating based on the manufacturer's specifications. Each joint was tested by dropping the respective link from a given angular position, and the joint angle data over time data was collected. The movement of each joint was isolated by locking out the other two joints for each respective test. This data, along with the updated leg geometrical properties, was run through a simple version of the optimization process outline in chapter two, where the viscous damping is optimized for, using the rise time as the cost calculation.

These new damping constants were then assigned as set variables and run through the optimization process once more with the desired scaled rat leg responses, to optimize for the spring constants that give the best responses given these damping parameters (Table 6). These new spring constants were used in the spring selection.

Parameter	Hip	Knee	Ankle
b desired (N-m-s/rad)	1.290	0.105	0.063
k desired (N-m/rad)	23.67	1.71	0.4538
b dampers (N-m-s/rad)	4.1056	0.0672	0.0277
k desired updated (N-m/rad)	79	2.2922	0.4646
k manufacturer (N-m/rad)	38	2.224743	0.47269

Table 6: Damping and spring constants as designed and actual manufacturer specs.

4.3.2 Spring design

The torsional springs for the knee and ankle were bought from a professional vendor to ensure spring quality and to avoid issues of plastic deformation [16]. When choosing springs, the goal was to find springs that were available in a 120-degree arm angle formation, were within 5% of the desired spring rate, and a body length and outside spring diameter of less than 1.25 inches, in order to keep the joint enlargement minimal (Table 7).

Specifications	Hip	Knee	Ankle
Vendor	In lab	Lee Springs	Lee Springs
Product number	n/a	LTR135H 10 M	LTR080F 10 S
Angle of arms	105 deg	120 deg	120 deg
Spring rate (N-m/rad)	38	2.2	0.47
Material	Music Wire	Music Wire	Type 302(SS)
Total coils	1.04	7.17	6.17
Wire diameter	0.188 in	0.135 in	0.080 in
Body length	0.6 in	1.1 in	0.52 in
Outside diameter	1.63	1.16 in	0.75 in

Table 7: Spring specifications.

A torsional spring was chosen to be made in house for the hip, as the range of motion is smaller for this joint, and plastic deformation is less of a concern. Additionally, a professionally made spring with the rate necessary for the hip would be quite large and create more of a design challenge to incorporate it into the hip joint. Music wire was used to form the torsional spring, due to accessibility and suitable elasticity. The relationship between the spring rate and spring characteristics is [17]:

$$k = \frac{d^4 E}{64DN}$$

Equation 7

Here d is the wire diameter, D is the mean spring diameter, and N is the number of coils. For ease of design, N was set to 1 plus a partial rotation (15 degrees to achieve the required unloaded spring position). Doing so, the wire diameter and mean spring diameter can be adjusted to the correct k value, as many hardware stores sell an adequate range of music wire. A wire diameter of 0.1875 in was chosen, with an inner spring diameter of 1.25 in. With an N value of 1.04, this produces a theoretical spring rate 38 N-m/rad. This value is considerably lower than our desired spring rate but still within a reasonable range. Had our damper selection been closer to the original desired value however, this value would be slightly higher than the necessary spring value.

This spring design for the hip will be considered a point of improvement in future continuations of this project, as fitting a professionally made spring in the hip joint requires much more of a design overhaul due to the spring size. It does however, give us a testable initial prototype from which improvements can be made.

Chapter 5: Prototype testing

5.1 Methods

Once all spring and dampers had been added to the leg, the assembled leg was tested to determine the actual spring and damping values acting on the leg. This was completed by recording the joint angle positional data over time for each joint, given varying initial positions (Fig 19). The joint was moved to the desired position, as recorded by its encoder, and then released while the time and joint angle values were recorded. In order to isolate each joint as much as possible, the knee and hip were held in a set position when testing the ankle, and the hip was held in a set position when testing the knee. All joints below were allowed to rotate freely and then response was recorded for those as well.

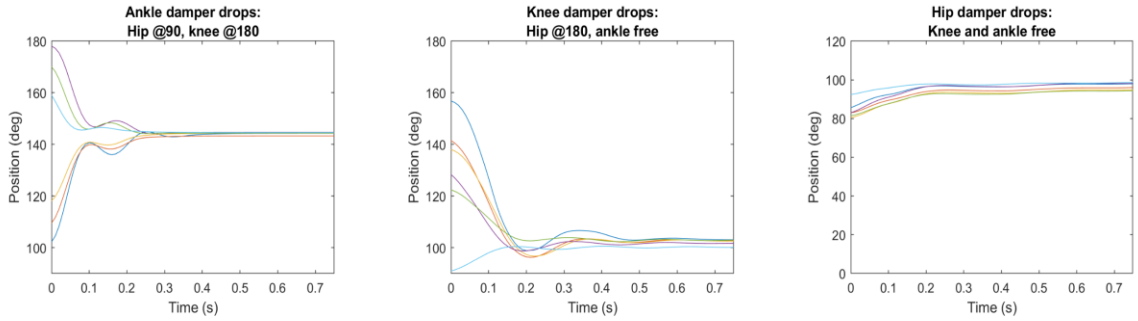

Figure 19: Data collected from each joint to establish actual spring and damping parameters on the robot leg.

A Nelder-Mead optimization was then run on each joint, beginning with the ankle, to solve for the damping and spring constant at each joint. The results for the ankle were then used in the simulation of the knee, as the ankle was allowed to rotate freely, and

both knee and ankle results were used in the hip simulations. The cost calculation used was the scaled sum of the difference in rise time, damping, and frequency in each trial between the actual collected data and the simulation data.

Additionally, the dynamics of the old leg design (without the spring and dampers) were visually compared to the new leg dynamics. This was completed by moving both legs to the same joint angle position, releasing the legs, and collecting encoder data over time. This was completed for two separate drops with different starting positions.

5.2 Results

Final damping and spring constants were recorded for all joints and simulated data based on the new model was compared to the experimental data of the joint responses (Fig 20, Table 8).

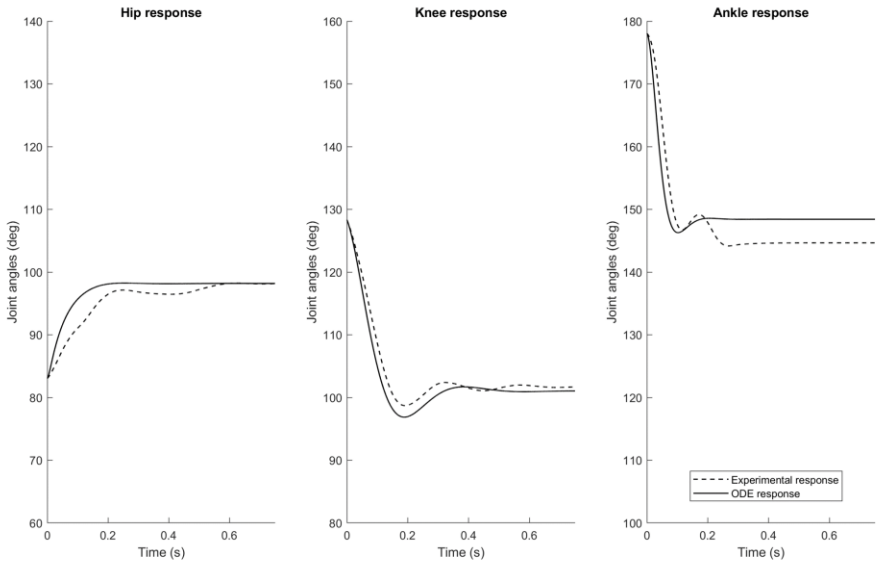

Figure 20: Three example trials (one of each joint) of isolated joint tests with simulated data created from optimization process.

Parameter	Hip	Knee	Ankle
Final damping constant (N-m-s/rad)	4.307	0.149	0.012
Final spring constant (N-m/rad)	75.794	2.288	0.361

Table 8: Results from parameter optimization of the isolated joint testing.

Graphs were created from the response data from the original leg, the novel leg, and the simulated leg based on the desired set of spring and damping parameters at two sets of starting positions (Fig 21).

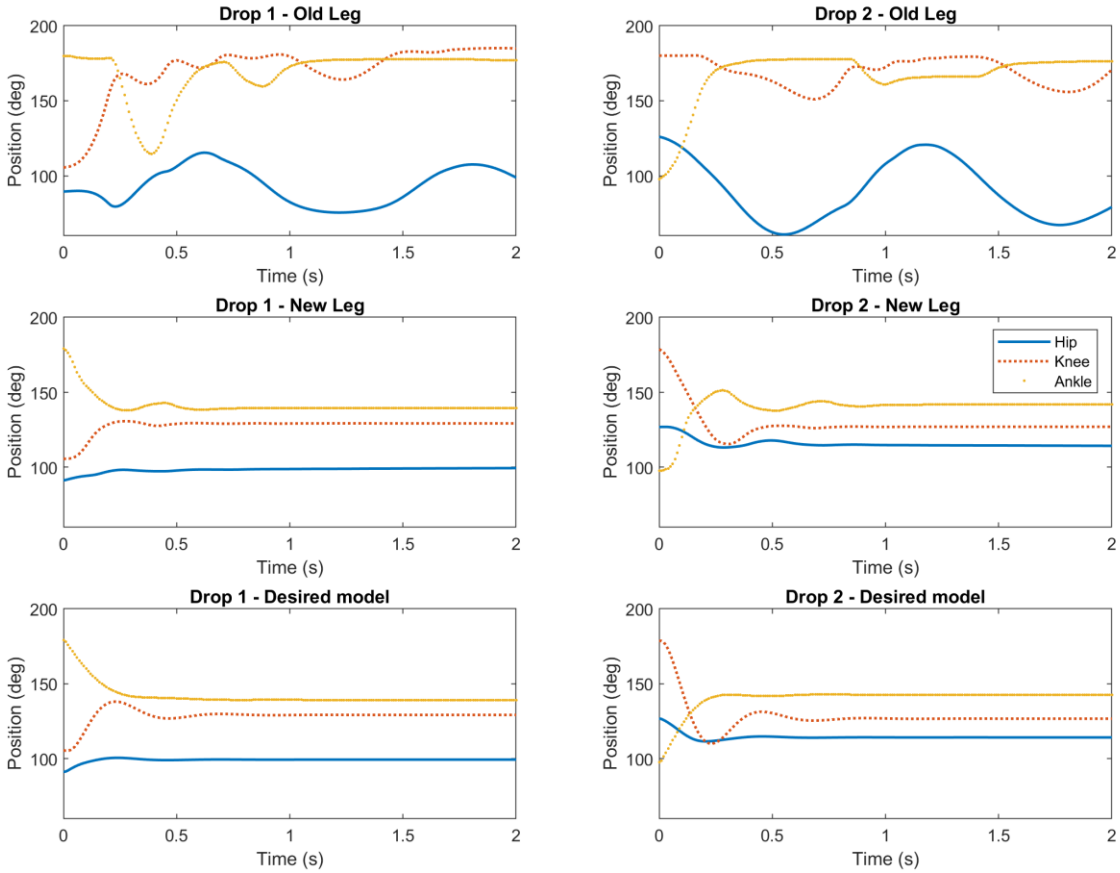

Figure 21: Test response data from old leg, new leg, and simulated leg based on parameters found in original scaled rat leg optimization.

5.3 Discussion

Comparing the responses of the old leg to the new leg, improvements have been made when considering all three joint responses. The old leg, only made a stable system by the presence of friction, clearly oscillates much more than you would expect from a rat (or a dog leg), and takes considerable time to fully settle (Fig 21). The novel leg increases the damping ratio and decreases the overshoot of all responses, creating a much more stable leg design.

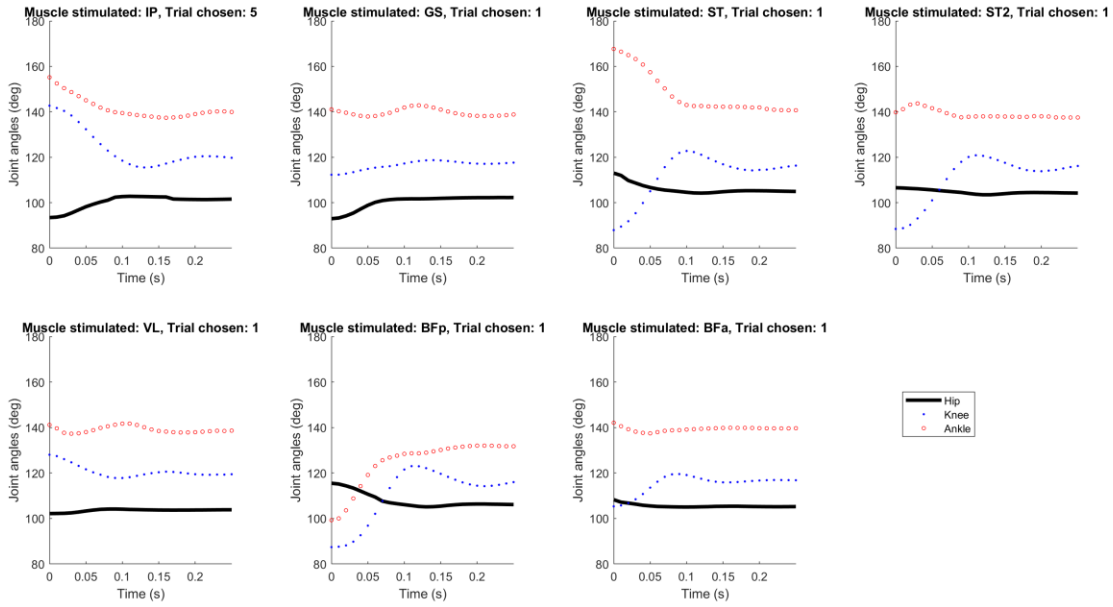

Figure 22: Kinematic data collected from the rat leg (unscaled).

From a qualitative perspective as well, the new leg positional response trials seem to mimic the overall response of the rat trials from a visual level (Fig 22). The oscillations in the hip are kept quite minimal, and the knee tends to oscillate only once or twice before settling. Similar to the observed response in the rat leg, the ankle exhibits less of a clean step response due to the effect of the joint movement from the knee and hip.

Unfortunately, the range of motion in the robot knee (approximately 0 to 80 degrees) prevents a direct comparison to the scaled rat leg responses. However, we can compare the new leg to the simulated response of our original desired model as found through the scaled rat leg optimization. There are observable similarities between the new leg and the simulated leg from the scaled rat leg oscillations (Fig 21). The hip joint now has a very comparable rise time to the desired model, with little overshoot, and the knee joint also responds on the same scale as the desired model and similar overshoot. The ankle appears to be less damped than the desired model, which was also a slight difference present between the simulated model and the actual rat leg data.

Chapter 6: Conclusions and future work

6.1 Rat leg passive dynamics mimicry

As a whole, the biomimicry of the leg has been improved. The passive dynamics of the new leg behave more like what is expected of a dog-sized quadruped. The leg now settles well under a second, while the previous leg oscillates for many cycles before coming to a halt, which does not resemble dog-leg behavior. With regard to the specific goal of creating a dog-sized robot leg with the scaled passive dynamics of a rat, this work suggests that it is possible to do so, but more iterations of the spring and damper parameter selection may be necessary to achieve a more accurate model. However, the passive dynamics of the rat are acquired by processing and analyzing data collected from trials where multiple joints are moved at once. This makes it more difficult to precisely determine the dynamics of the rat leg at each individual joint. Collecting data on one isolated joint at a time would improve the accuracy of the analysis, and thus increase confidence in the results.

6.2 Modeling discussion

There are several limitations that should be addressed in this study. First, these results can only be as accurate as the model it is based on. In this case, our leg has been simplified to three planar links, each with a single degree of freedom. The lateral movements of the hip and ankle have been eliminated in our current model, and it is not clear to what extent spring and viscous damping parameters can mimic the mechanical

behavior of the rather complex interaction of bone, musculature, and other soft tissue in the rat limb. This is a more difficult question to address and will be interrogated further in future studies.

Another simplification that has been made is the lack of Coulomb damping. Due to the scope and time constraints of this project, the presence of friction was not accounted for in our model. Although the recent modification of adding steel rods acting as rotary shafts at each joint has reduced friction occurring with angular rotation, friction cannot be eliminated in the robot leg and should be accounted for. Preliminary modeling included the effects of friction, but resulted in long run times and was eliminated from the process. This should be revisited with a more thorough process in modeling Coulomb damping. As discussed in chapter five, the addition of the torsion springs has also introduced a non-negligible amount of Coulomb damping, and the system model should be updated to reflect this.

Although the system model does include viscous damping, it should be noted that most rotary dampers do not actually have a strictly linear relationship of torque exerted and rotational speed, as is assumed initially in this project. Additionally, most dampers do not have the same non-linear relationship between these variables either, compounding the difficulty of the problem. One potential solution for streamlining this process in the future is to create a damping model for a damper with an adjustable damping constant as a function of speed, eliminating the need to re-adjust the damping parameter every time a different rotary damper is used.

6.3 Design improvements

The design of the knee and ankle was successful in that the joints were kept the same fundamental design as the original leg (while adding minimal extra mass), do not protrude out of the plane of the leg to any major extent, and are relatively easy to disassemble and adjust (Fig 23). The re-design of the hip with the spring implementation however, should be a future point of design improvement.

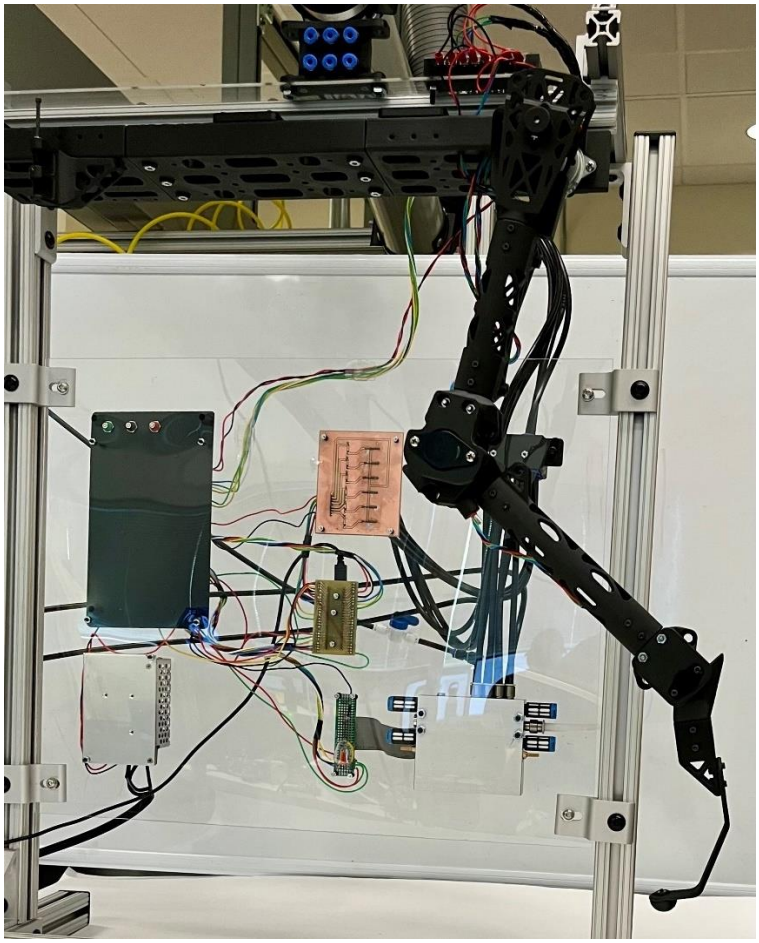

Figure 23: Completed and assembled leg on the quadruped test bench.

The issue of the hip spring could be addressed in one of three ways. First, a larger stock torsion spring could be used, and would likely be much higher quality than could be made ourselves. This would require a more significant overhaul of the joint, due to the likely size of a spring of that strength.

Second, a custom-made spring could be ordered. The drawbacks for this would be time and financial cost. If iterations of the design need to be made, waiting for a custom spring order will take longer than purchasing stock springs. However, it would provide an advantage in that a smaller number of coils could be designated, allowing for the spring to fit in the joint without a more significant re-design.

Third, instead of ordering a custom-made spring, a more effective spring-building process could be established, allowing the AARL to make a spring according to our own specifications. This would require establishment of a spring forming process that can reliably produce expected spring rates, including heat-treatment of the formed spring.

6.4 Modularity in workflow

As it is an objective of the AARL to test the functionality of multiple leg systems that vary in dynamic behavior with different types of SNS control, it is likely that variations of this novel leg system will eventually be drafted and/or built. One ideal outcome of this project would be to establish a process in which any desired system can be designed with a streamlined workflow. As in, if adequate data and mechanical properties are known about a given limb, a user could simply input this data with minimal modification to

existing code, and be given a set of spring and damping parameters as an output (to be implemented on a robot limb).

Though this project is certainly a step in that direction, more improvements will need to be made to make that a reality, some of which are outlined above. The biggest step towards a more universal pipeline for this is to create a set of cost functions that are effective regardless of the characteristics of the response data collected. The cost calculations used in this study were more tailored to known data sets (i.e., using rise time to for hip parameters, as it appears to be overdamped, or using frequency and damping for the knee as it behaves more like an isolated second order system). If the scope of this project were larger this could potentially be achieved by creating an array of hypothetical leg systems and testing the validity of the optimization on theoretical data.

Although there is no shortage of developments to be made on the passive dynamic modeling workflow and current design of the scaled rat leg, this will hopefully lay a solid foundation for continuing research. This work should serve as starting blocks for the design of a more comprehensive set of legs with distinctly different dynamic behavior, and for more extensive research on synthetic nervous systems and their relationship with the physical system of the limb, primarily as applied in locomotion.

Bibliography

[1] C. Scharzenberger and A. Hunt, “A Functional Subnetwork Approach to Multistate Central Pattern Generator Phase Difference Control (Short),” p. 12.

[2] A. J. Ijspeert, “A connectionist central pattern generator for the aquatic and terrestrial gaits of a simulated salamander,” *Biol. Cybern.*, vol. 84, no. 5, pp. 331–348, Apr. 2001, doi: 10.1007/s004220000211.

[3] W. W. Hilts, N. S. Szczecinski, R. D. Quinn, and A. J. Hunt, “A Dynamic Neural Network Designed Using Analytical Methods Produces Dynamic Control Properties Similar to an Analogous Classical Controller,” p. 6, 2018.

[4] T. Buschmann, A. Ewald, A. von Twickel, and A. Büschges, “Controlling legs for locomotion—insights from robotics and neurobiology,” *Bioinspir. Biomim.*, vol. 10, no. 4, p. 041001, Jun. 2015, doi: 10.1088/1748-3190/10/4/041001.

[5] M. H. Dickinson, C. T. Farley, R. J. Full, M. a. R. Koehl, R. Kram, and S. Lehman, “How Animals Move: An Integrative View,” *Science*, vol. 288, no. 5463, pp. 100–106, Apr. 2000, doi: 10.1126/science.288.5463.100.

[6] C. W. Scharzenberger, “Design of a Canine Inspired Quadruped Robot as a Platform for Synthetic Neural Network Control,” Portland State University, 2019.

[7] “Onyx 3D Printer Filament and Printing Material | Markforged,” *Markforged*. https://markforged.com/materials/onyx/ (accessed Apr. 26, 2019).

[8] K. S. Aschenbeck, N. I. Kern, R. J. Bachmann, and R. D. Quinn, “Design of a Quadruped Robot Driven by Air Muscles,” *First IEEERAS-EMBS Int. Conf. Biomed. Robot. Biomechatronics*, pp. 875–880, 2006, doi: 10.1109/BIOROB.2006.1639201.

[9] Gregory Sutton, Roger Quinn, Nicholas Szczecinski, and Hillel Chiel, “Neural control of rhythmic limb motion is shaped by size and speed”.

[10] “(PDF) A New Approach to Assess the Gastrocnemius Muscle Volume in Rodents Using Ultrasound; Comparison with the Gastrocnemius Muscle Index.” https://www.researchgate.net/publication/234159106_A_New_Approach_to_Assess_the_Gastrocnemius_Muscle_Volume_in_Rodents_Using_Ultrasound_Comparison_with_the_Gastrocnemius_Muscle_Index (accessed Oct. 24, 2022).

[11] K. Lynch and F. Park, *Modern Robotics: Mechanics, Planning, and Control*. Cambridge U. Press, 2017. [Online]. Available: http://modernrobotics.org

[12] J. Sammartino, “Dynamic Scaling of a Dog Robot.” Portland State University, Aug. 2021.

[13] J. Kennedy and R. Eberhart, “Particle Swarm Optimization,” *Proc. ICNN95 - Int. Conf. Neural Netw.*, 1995, [Online]. Available: https://doi.org/10.1109/icnn.1995.488968

[14] W. T. Kano *et al.*, “Kinetic and temporospatial gait parameters in a heterogeneous group of dogs,” *BMC Vet. Res.*, vol. 12, no. 1, p. 2, Jan. 2016, doi: 10.1186/s12917-015-0631-2.

[15] “ACE Rotary Damper Catlogue.” ACE Controls Inc. Accessed: Oct. 25, 2022. [Online]. Available:

https://www.acornbearings.co.uk/downloads/catalogues/aerospace/struts-and-dampers/ace-rotary-dampers.pdf

[16] "Torsion Springs," *LeeSpring*. https://www.leespring.com/torsion-springs

[17] *FE Reference Handbook*, 10.1. NCEES, 2020.

Appendix A: Final error for scaled rat leg response optimized parameters

	Trial 1	Trial 2	Trial 3	Trial 4	Trial 5	Trial 6	Trial 7	Avg err	Avg err of weighted trials
Desired hip risetime	0.104	0.134	0.108	0.150	0.066	0.122	0.098		
Actual hip risetime	0.068	0.1	0.108	0.042	0.056	0.08	0.022		
Error	35%	25%	0%	72%	15%	34%	78%	37%	20%
Desired knee omega	18.5	7.6	17.8	14.2	23.8	16.4	22.8		
Actual knee omega	13.8	15.2	13.8	13.7	13.8	14.0	25.5		
Error	25%	101%	22%	3%	42%	15%	12%	32%	16%
Desired knee zeta	0.378	0.309	0.443	0.375	0.311	0.375	0.474		
Actual knee zeta	0.384	0.303	0.388	0.390	0.384	0.381	0.226		
Error	2%	2%	12%	4%	23%	2%	52%	14%	5%
Average joint angle difference ankle	-0.42	-0.92	-1.24	-0.99	-0.50	-0.18	-0.35	-0.66	

Table A- 1: Individual trial data on desired and achieved passive dynamic characteristics.

Appendix B: Trials used in calculation of actual robot leg spring and damper values

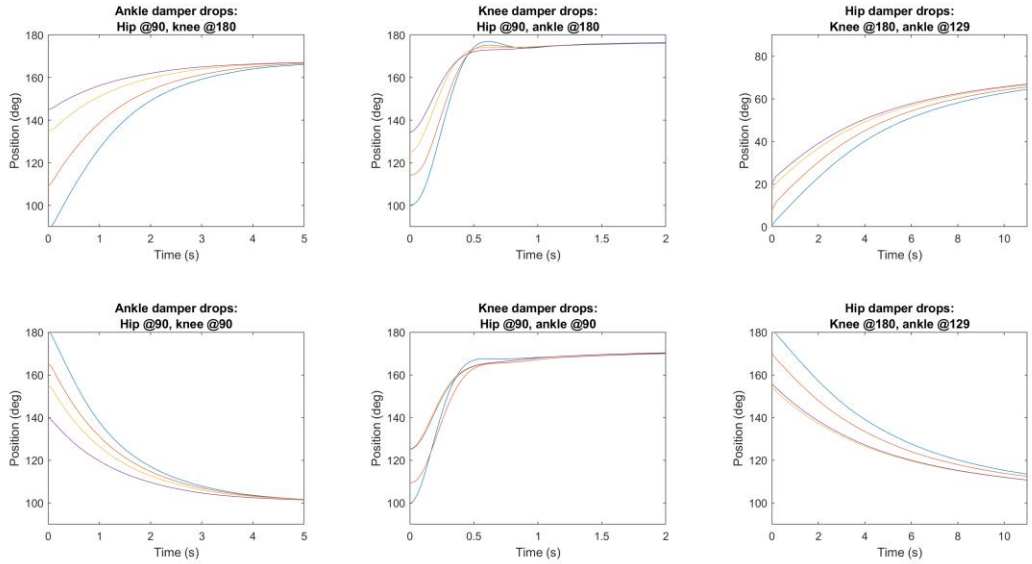

Figure B- 1: Trials used for initial damping calculations of robot joints.

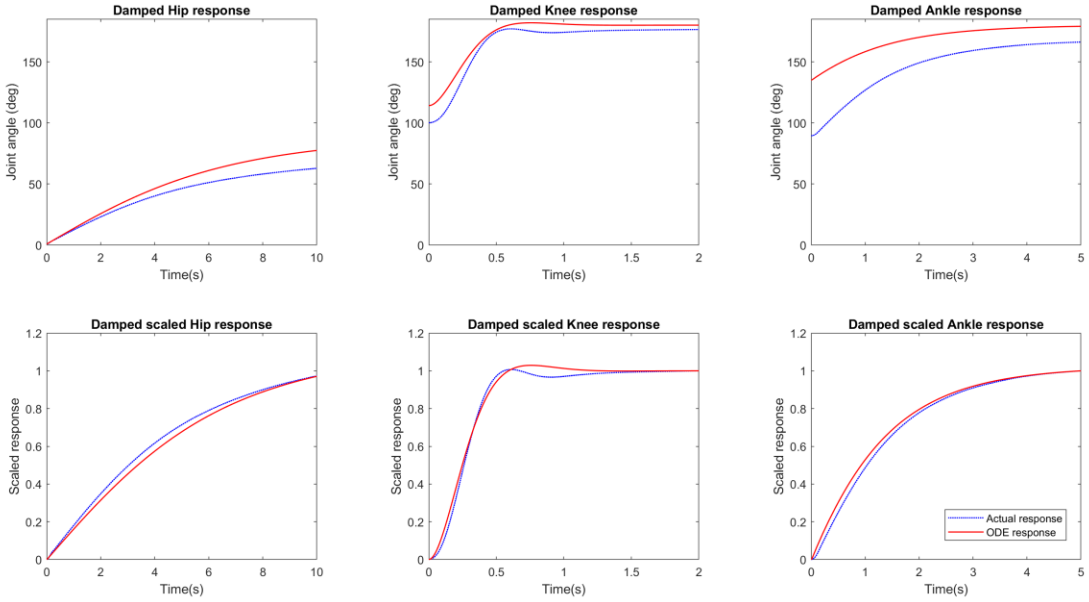

Figure B- 2: Modeled and actual damped responses of joints with dampers only.

Appendix C: CAD drawings of spring, damper, and joint pieces

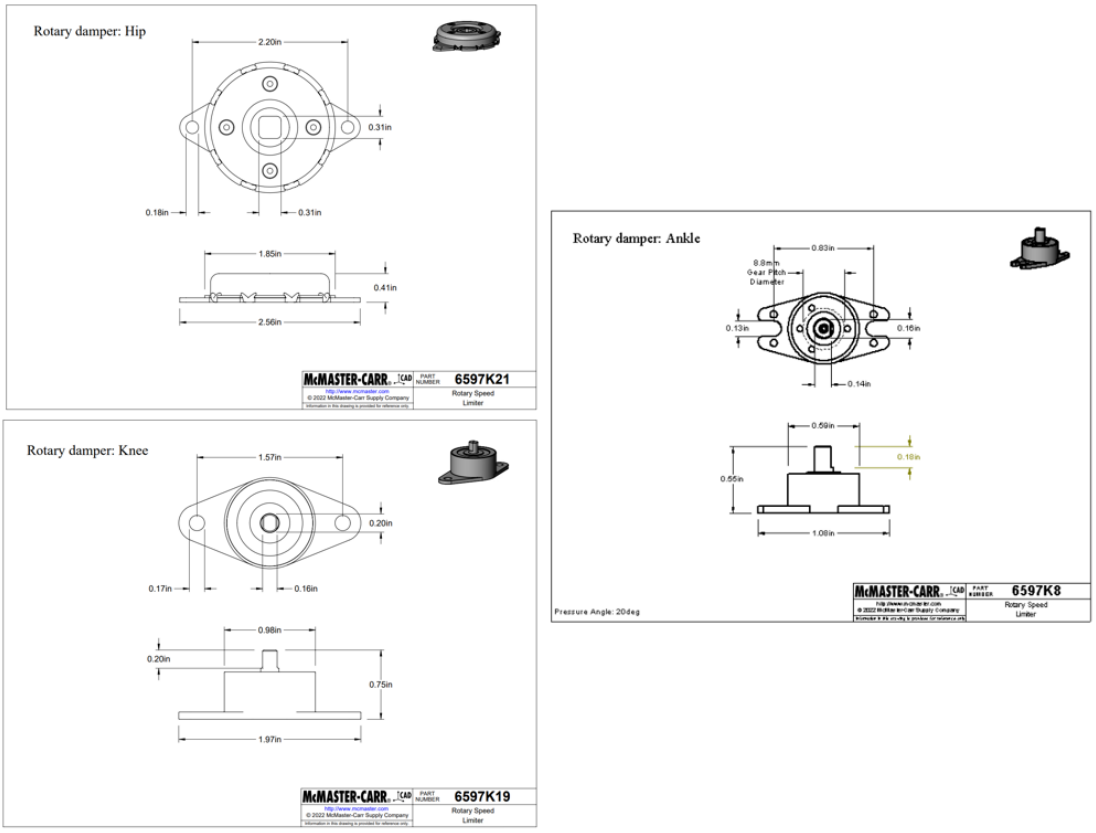

Figure C- 1: CAD drawings of dampers used and purchased from McMaster-Carr.

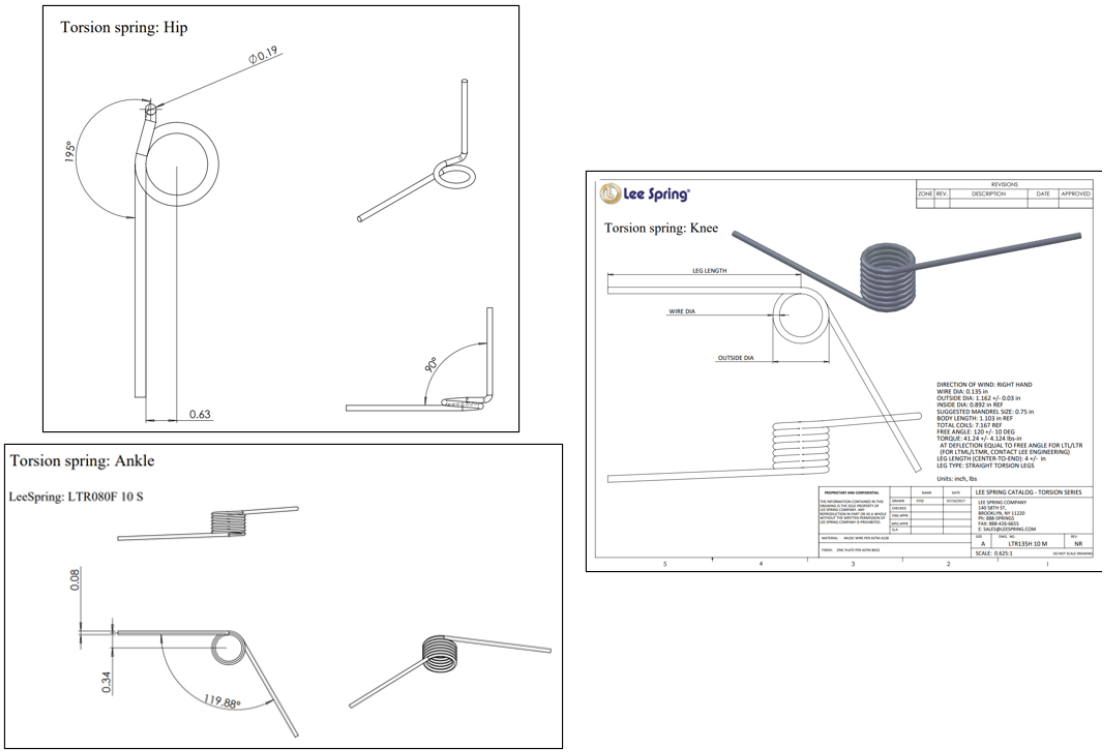

Figure C- 2: CAD drawings for torsional springs used.

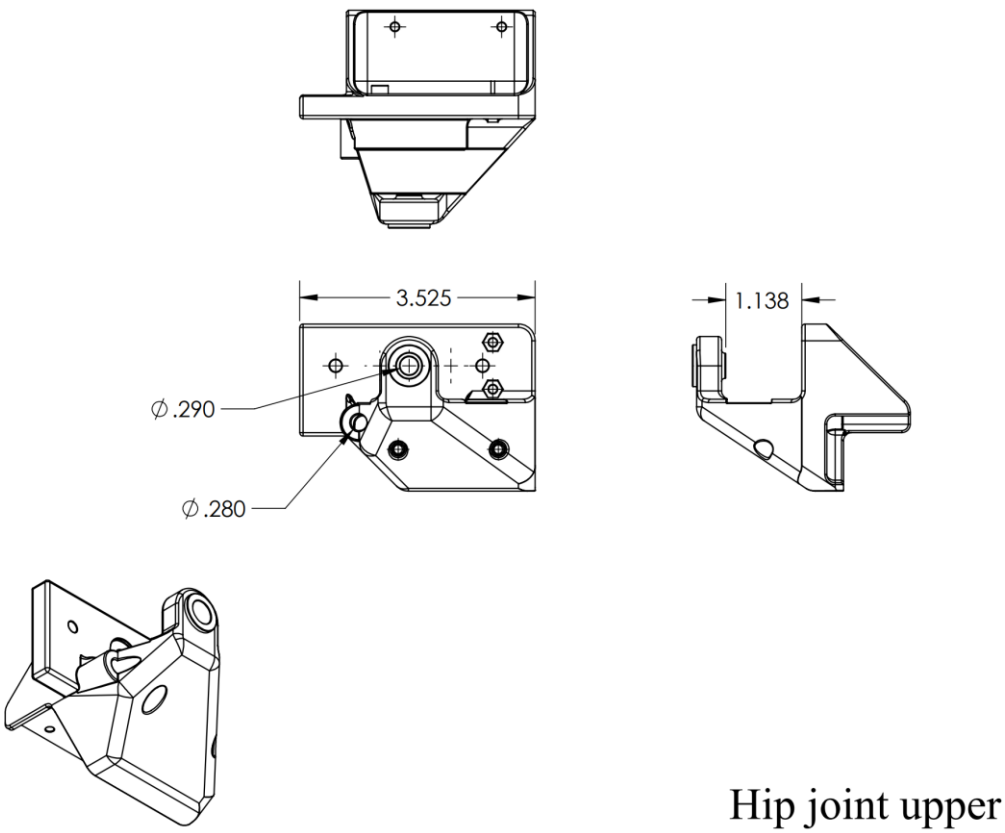

Figure C- 3: CAD drawing of upper hip joint piece.

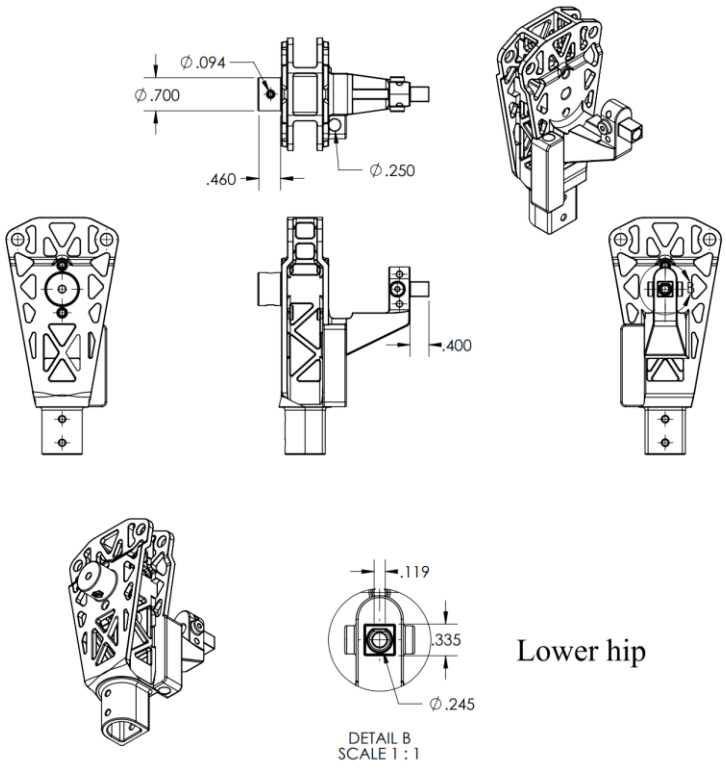

Figure C- 4: CAD drawing of lower hip joint piece.

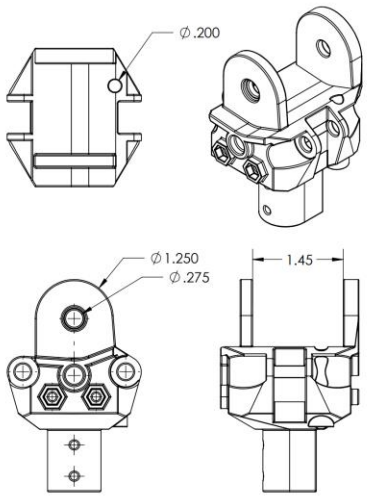

Knee joint upper

Figure C- 5: CAD drawing of upper knee joint piece.

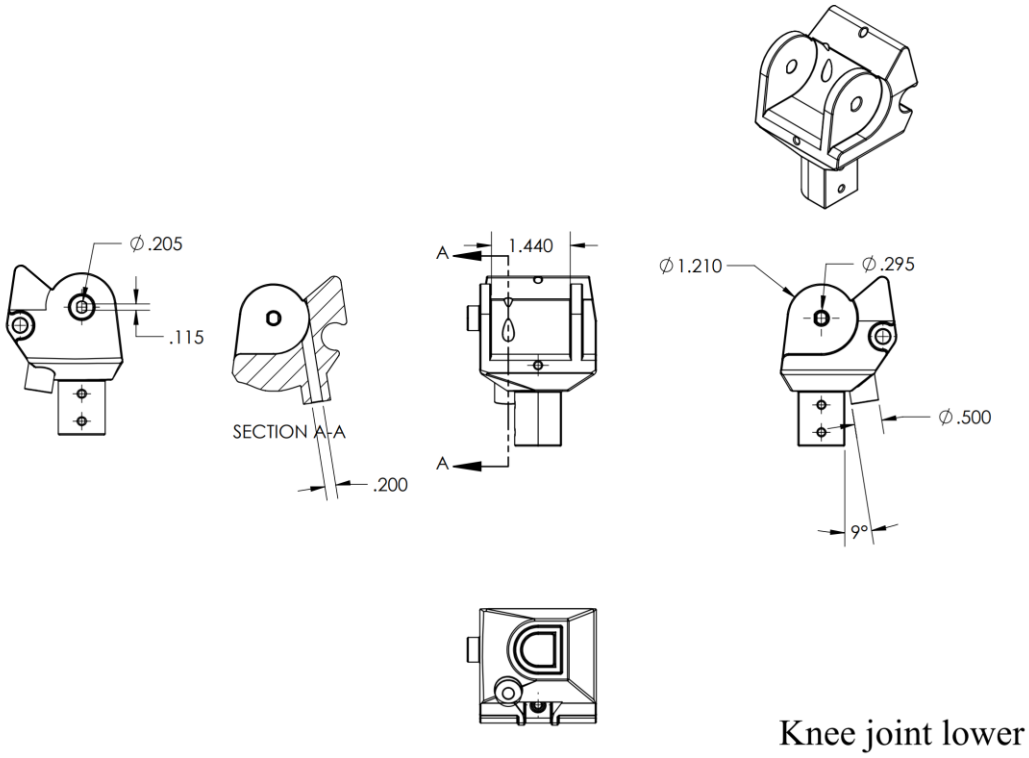

Knee joint lower

Figure C- 6: CAD drawing of lower knee joint piece.

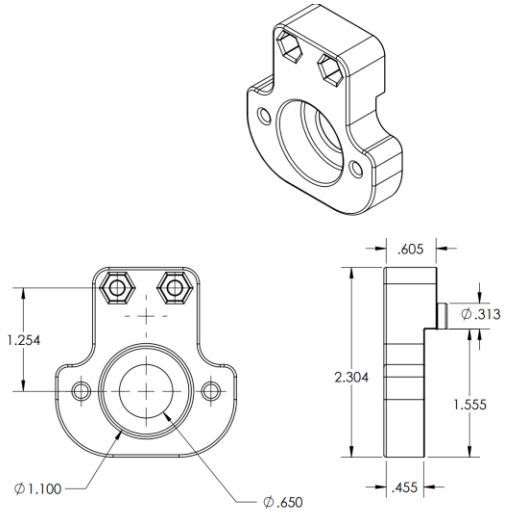

Figure C- 7: CAD drawing of knee damper bracket.

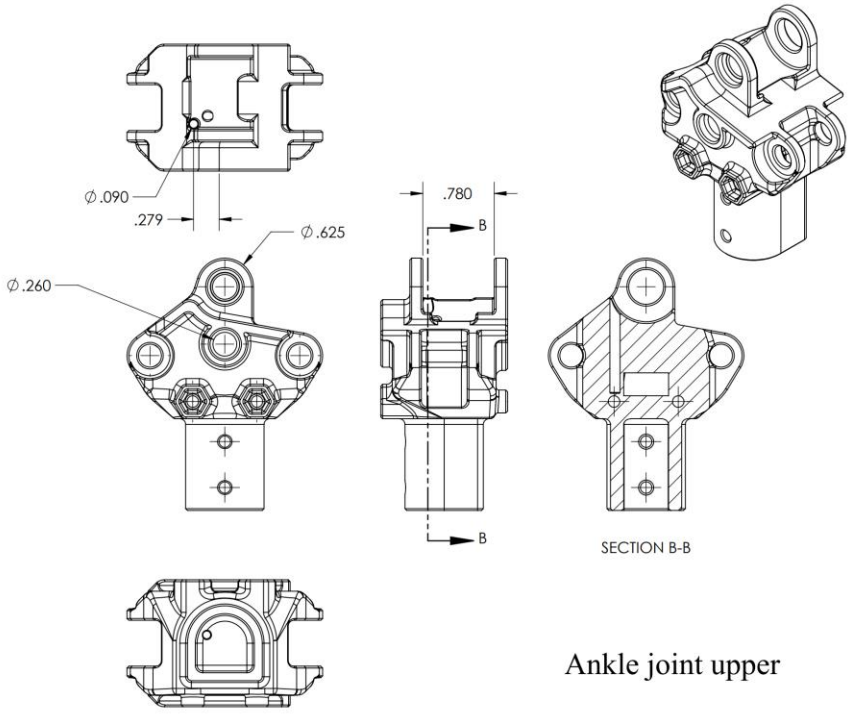

Figure C- 8: CAD drawing of upper ankle joint piece.

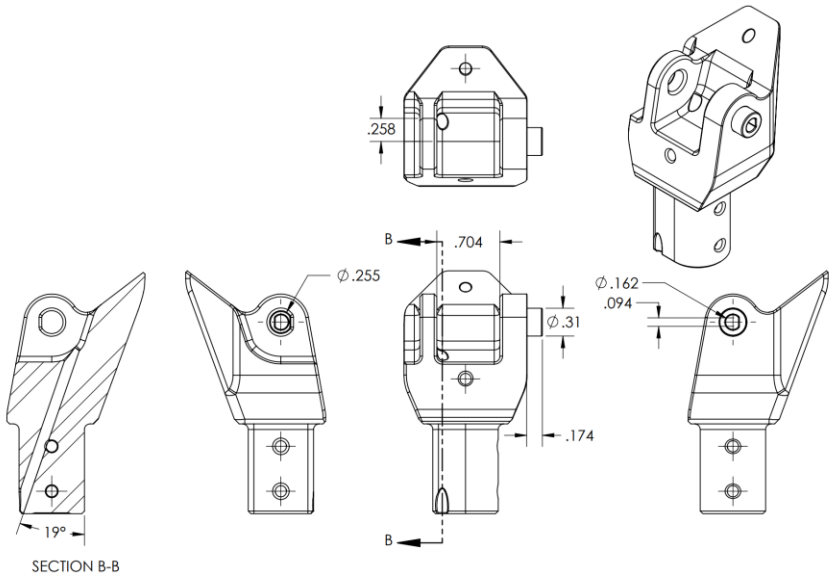

Figure C- 9: CAD drawing of lower ankle joint piece.

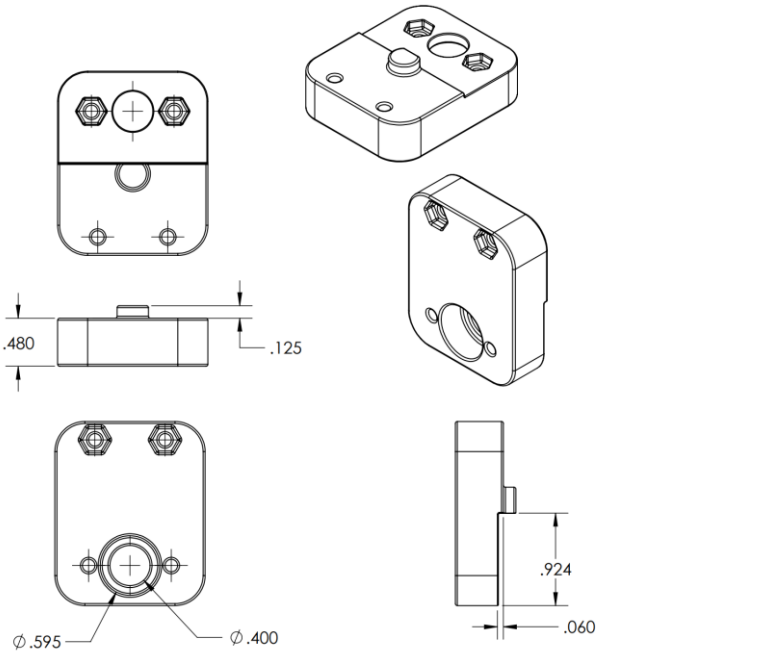

Figure C- 10: CAD drawing of bracket for ankle joint damper.